Title

Epidermal growth factor augments the self-renewal capacity of aged hematopoietic stem cells.

Journal

iScience, 27(7)

Authors

Chang, Vivian
He, Yuwei
Grohe, Samantha
et al.

Publication Date

2024-07-19

DOI

10.1016/j.isci.2024.110306

Peer reviewed

iScience

CellPress
OPEN ACCESS

Article

Epidermal growth factor augments the self-renewal capacity of aged hematopoietic stem cells

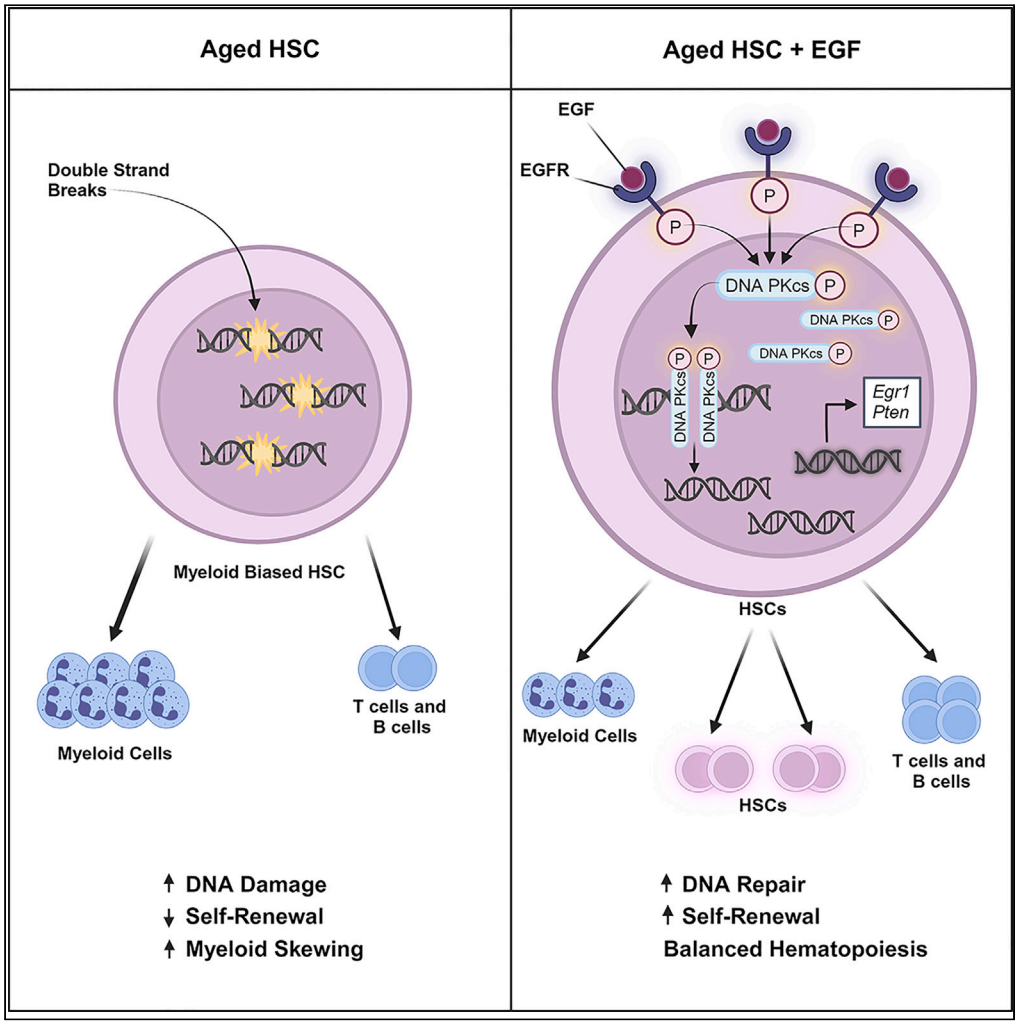

Vivian Y. Chang, Yuwei He, Samantha Grohe, ..., Heather A. Himburg, Peibin Yue, John P. Chute

john.chute@cshs.org

Highlights

Aged, myeloid-biased HSCs display increased EGFR expression

EGF augments the self-renewal capacity of aged HSCs

EGF amplifies DNA repair and self-renewal programs in aged HSCs

EGFR deletion decreases HSC self-renewal in middle aged mice

Chang et al., iScience 27, 110306
July 19, 2024
https://doi.org/10.1016/j.isci.2024.110306

iScience

CellPress
OPEN ACCESS

Article

Epidermal growth factor augments the self-renewal capacity of aged hematopoietic stem cells

Vivian Y. Chang,[1,2,3] Yuwei He,[4] Samantha Grohe,[4] Morgan R. Brady,[4] Aldi Chan,[4] Rucha S. Kadam,[4] Tiancheng Fang,[5] Amara Pang,[6] Katherine Pohl,[6] Evelyn Tran,[6] Michelle Li,[6] Jenny Kan,[6] Yurun Zhang,[7] Josie J. Lu,[8] Joshua P. Sasine,[4] Heather A. Himburg,[9] Peibin Yue,[4] and John P. Chute[4,10,11,12,13,*]

SUMMARY

Hematopoietic aging is associated with decreased hematopoietic stem cell (HSC) self-renewal capacity and myeloid skewing. We report that culture of bone marrow (BM) HSCs from aged mice with epidermal growth factor (EGF) suppressed myeloid skewing, increased multipotent colony formation, and increased HSC repopulation in primary and secondary transplantation assays. Mice transplanted with aged, EGF-treated HSCs displayed increased donor cell engraftment within BM HSCs and systemic administration of EGF to aged mice increased HSC self-renewal capacity in primary and secondary transplantation assays. Expression of a dominant negative EGFR in Scl/Tal1^{+} hematopoietic cells caused increased myeloid skewing and depletion of long term-HSCs in 15-month-old mice. EGF treatment decreased DNA damage in aged HSCs and shifted the transcriptome of aged HSCs from genes regulating cell death to genes involved in HSC self-renewal and DNA repair but had no effect on HSC senescence. These data suggest that EGFR signaling regulates the repopulating capacity of aged HSCs.

INTRODUCTION

Hematopoietic stem cell (HSC) numbers increase in mammals with age in what is considered a compensatory response to their decreased ability to engraft and differentiate.[1,2] As HSCs age, they display distinct abnormalities such as skewing toward myeloid differentiation, decreased repopulating capacity, and leukemia susceptibility.[1,3] Clinically, this corresponds with an increasing incidence of myelodysplasia, acute leukemia, as well as immune system defects,[4–7] contributing to significant morbidity and mortality for the aging population.

Cell-intrinsic processes regulate HSC function during aging, including mitochondrial stress response,[8,9] autophagy,[10] regulation of polarity,[11] and DNA repair mechanisms.[12,13] Several studies have demonstrated that HSCs accumulate DNA damage with aging[12,14,15] and deficiencies in nucleotide excision repair, telomere maintenance, and non-homologous end-joining (NHEJ) caused a severe loss in HSC self-renewal capacity and functional exhaustion with age.[12] The quiescence of aging HSCs promotes accrual of DNA damage, which is promptly repaired upon induction of aged HSCs into cell cycle.[14] Gutierrez-Martinez et al. showed further that aged HSCs display diminished ATM function and DNA damage response, leading to increased clonal survival that may contribute to mutation accrual in aged HSCs.[16]

Aging of bone marrow (BM) niche components, including vascular and perivascular stromal cell niches,[17,18] skeletal stem cells that drive a pro-inflammatory BM niche,[19,20] and deterioration in adrenergic nerve function,[20] have also been shown to contribute to hematopoietic decline with aging. Additional studies have suggested that a decline in mTOR signaling in BM endothelial cells (BM ECs) may specifically promote aging of hematopoietic stem/progenitor cells.[21] Furthermore, infusion of young ECs into aged mice partially rescued HSC repopulating capacity compared to that of aged control mice,[22] and treatment of aged HSCs with BM stromal cell-derived osteopontin, whose expression decreases with aging, reestablished lymphoid-myeloid balance and polarity of aged HSCs.[22,23] Similarly, BM stromal cell-derived

[1]Division of Hematology-Oncology, Department of Pediatrics, UCLA, Los Angeles, CA, USA
[2]Children's Discovery and Innovation Institute, UCLA, Los Angeles, CA, USA
[3]Jonsson Comprehensive Cancer Center, UCLA, Los Angeles, CA, USA
[4]Division of Hematology & Cellular Therapy, Cedars Sinai Medical Center, Los Angeles, CA, USA
[5]Department of Molecular and Medical Pharmacology, UCLA, Los Angeles, CA, USA
[6]Division of Hematology/Oncology, Department of Medicine, University of California, Los Angeles, Los Angeles, CA, USA
[7]Molecular Biology Institute, UCLA, Los Angeles, CA 90095, USA
[8]Applied Genomics, Computation and Translational Core, Cedars Sinai Medical Center, Los Angeles, CA, USA
[9]Department of Radiation Oncology, Medical College of Wisconsin, Milwaukee, WI, USA
[10]Board of Governors Regenerative Medicine Institute, Cedars Sinai Medical Center, Los Angeles, CA 90095, USA
[11]Samuel Oschin Cancer Center, Cedars Sinai Medical Center, Los Angeles, CA 90095, USA
[12]Department of Medicine, Cedars Sinai Medical Center, Los Angeles, CA 91361, USA
[13]Lead contact
*Correspondence: john.chute@cshs.org
https://doi.org/10.1016/j.isci.2024.110306

IL-1 signaling was shown to contribute to an inflammatory niche that drives hematopoietic aging,[24] whereas a decline in BM stromal cell production of IGF1 was also associated with accelerated hematopoietic aging in mice.[25] Ramalingam et al. reported that administration of Netrin 1 to aged mice improved BM vascular niche cell DNA repair and restored vascular niche function in association with rescue of HSC self-renewal capacity.[26] Taken together, these studies demonstrate that BM microenvironment mechanisms regulate hematopoietic aging. However, recent studies have also shown that a young BM microenvironment has limited capacity to rejuvenate old transplanted HSCs[27] and bloodborne factors are unable to restore function to aged HSCs.[28] Durable rejuvenation of aged HSCs may require correction of epigenomic changes which occur as HSCs age and which likely affect HSC self-renewal and differentiation capacities.[29–31]

We recently reported that epidermal growth factor (EGF), which is expressed by BM ECs,[32,33] promoted NHEJ repair in HSCs following chemotherapy or total body irradiation (TBI) stress and that EGF treatment promoted restoration of the self-renewal capacity of young HSCs following irradiation in a DNA-PKcs-dependent manner.[34] Separately, RNA sequence analysis of BM hematopoietic cells from middle-aged mice suggested that a decline in EGF signaling was associated with hematopoietic aging.[25] We hypothesized that activation of EGF-EGFR signaling might restore some functions of aged HSCs. Here, we report that EGF treatment *in vitro* or *in vivo* increased the self-renewal capacity of aged HSCs while shifting the HSC transcriptome to enrichment for genes involved with HSC self-renewal and specification. Hematopoietic cell-specific deletion of EGFR decreased long term-HSC (LT-HSC) function as measured in secondary transplantation assays. These results suggest that augmentation of EGFR signaling regulates HSC repopulating capacity in aged HSCs.

RESULTS

Expression of EGF and EGFR in the hematopoietic system of aged mice

For all experiments, we defined aged mice as *C57BL/6* mice, 18–22 months old, in keeping with prior studies.[35,36] We first compared EGF levels and EGFR functional activity in aged mice compared to young mice (6–8 weeks). While serum EGF levels were not different between aged and young mice, EGF levels were significantly increased in the BM of aged mice (Figure 1A). The concentrations of other EGFR ligands, betacellulin, and heparin binding EGF-like growth factor, were not different in the BM of aged versus young mice (Figure S1A). EGFR expression by RT-qPCR in BM $CD34^{-}ckit^{+}sca\text{-}1^{+}lineage^{-}$ ($34^{-}KSL$) cells, which are enriched for HSCs,[37] was not significantly different between aged and young mice (Figure 1B). However, EGFR surface expression was significantly increased on BM $34^{-}KSL$ HSCs in aged mice compared to young mice and a higher percentage of aged HSCs expressed surface EGFR than young mice (Figures 1C and 1D). EGFR expression was also significantly increased on $CD229^{-}CD150^{+}CD48^{-}KSL$ myeloid biased HSCs (MB-HSCs) in aged mice compared to young mice (Figures 1E and 1F) and $EGFR^{+}$ HSCs were enriched for MB-HSCs in aged mice compared to young mice (Figures S1B–S1E).

Functionally, aged HSCs displayed significantly increased phosphorylation of EGFR Y1173 residue at baseline compared to young HSCs (Figures 1G and 1H). In response to 20 ng/mL EGF treatment, young HSCs significantly increased phosphorylation of Y1173 EGFR, whereas aged HSCs also increased phosphorylation of Y1173, but not significantly (Figures 1G and S1F). In response to higher EGF concentration (100 ng/mL), aged HSCs significantly increased phosphorylation of Y1173, whereas young HSCs displayed no response (Figures 1H and S1G). Phosphorylation of the Y1068 EGFR increased in young HSCs in response to EGF treatment, whereas aged HSCs showed a non-significant trend toward increased phosphorylation (Figure S1H).

EGF treatment decreases DNA damage in aged HSCs

Aged HSCs have been shown to accumulate increased DNA damage compared to young HSCs[12,14,15] and defects in homologous recombination (HR) or NHEJ have been shown to cause severe deterioration in HSC self-renewal capacity.[12] Our lab has demonstrated that EGFR pathway activation decreases DNA damage in young HSCs following irradiation via activation of NHEJ repair.[34] We sought to evaluate whether EGFR activation could augment DNA repair in aged HSCs. We isolated BM $34^{-}KSL$ HSCs[37] from aged and young mice and compared the frequencies of γ-H2AX foci, which indicate sites of double-stranded DNA breaks.[13] Aged HSCs demonstrated increased MFI of γ-H2AX compared to young HSCs (Figure 2A). Aged HSCs also displayed increased DNA damage via the Comet assay, which detects DNA strand breaks as tail moments,[38] compared to young HSCs (Figure 2B). Treatment of aged HSCs in complete culture media supplemented with thrombopoietin (20 ng/mL), stem cell factor (125 ng/mL) and Flt3 ligand (50 ng/mL)(Media) with EGF x 2 h significantly decreased the percentages of $\gamma\text{-}H2AX^{+}$ HSCs and tail moment lengths in aged HSCs compared to aged HSCs cultured in Media + PBS (Figures 2C and 2D). Confocal microscopy confirmed increased numbers of γ-H2AX foci in aged HSCs compared to young HSCs cultured in media alone and demonstrated that EGF treatment decreased γ-H2AX foci in aged HSCs (Figure S2A).

Aged HSCs and young HSCs displayed comparable phosphorylation of DNA-dependent protein kinase-catalytic subunit (DNA-PKcs), the nuclear enzyme required for ligation and processing of DNA double-strand breaks during NHEJ,[39,40] (Figure 2E). Treatment with EGF increased phospho-DNA-PKcs levels at 5 min in aged HSCs compared to aged HSCs cultured in Media alone, but p-DNA-PKcs levels rapidly declined at 15 min and 30 min, returning to levels detected in HSCs from young mice. EGF treatment also increased phosphorylation of Artemis, the principal NHEJ endonuclease which complexes with and is activated by DNA-PKcs during NHEJ repair (Figure 2F),[41] but p-Artemis levels also declined at 15 min and 30 min to that observed in HSCs from young mice. EGF treatment × 72 h had no significant effect on the cell cycle status of BM $34^{-}KSL$ cells or the percentages of apoptotic or necrotic $34^{-}KSL$ cells in culture (Figures S2B and S2C). EGF treatment also had no effect on levels of SA-β-galactosidase, a marker of cell senescence,[42] or reactive oxygen species,[43] which characteristically accumulate in aged HSCs (Figures S2D and S2E).

Colony forming cell assays revealed that aged BM $34^{-}KSL$ cells produce increased total colonies and increased numbers of colony forming unit-granulocyte monocyte (CFU-GMs) compared to young BM $34^{-}KSL$ cells (Figure 2G). Aged HSCs treated with EGF demonstrated

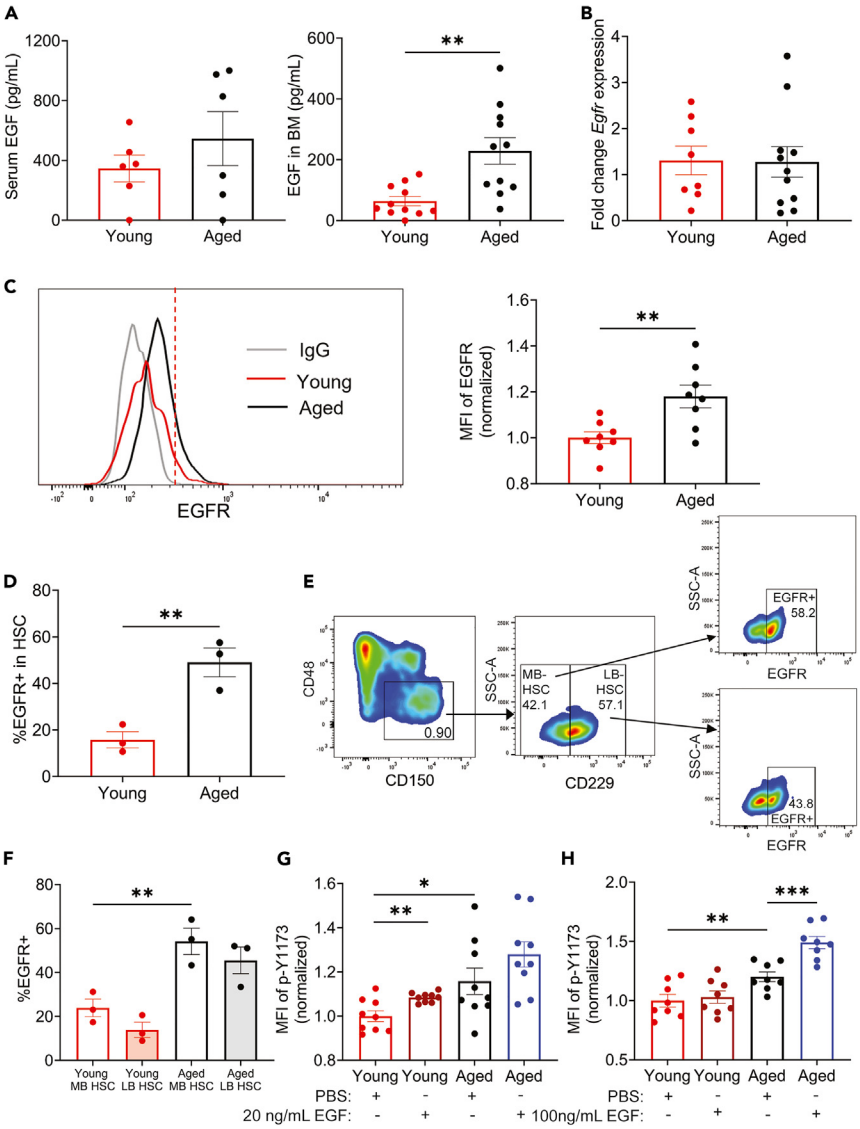

Figure 1. Expression of EGF and EGFR increases in the aged hematopoietic system

(A) At left, EGF levels in serum of young and aged mice (n = 6/group, t test); at right, EGF levels in the BM (n = 11/group, t test).

(B) *Egfr* expression by RT-qPCR in BM 34$^-$KSL cells from young and aged mice (n = 8–11/group).

(C) At left, representative histogram of EGFR surface expression on BM 34$^-$KSL cells from young and aged mice. At right, mean fluorescence intensity (MFI) of EGFR on BM34$^-$KSL cells in each group (n = 8/group, t test).

(D) %EGFR$^+$ BM CD150$^+$CD48$^-$ (SLAM) KSL HSCs in young and aged mice (n = 3/group, t test).

(E) Representative flow cytometric analysis of EGFR$^+$ and EGFR$^-$ cells within the CD229$^-$ SLAM KSL HSCs (MB-HSC) and CD229$^+$ SLAM KSL HSCs (LB-HSC).

(F) Mean %EGFR$^+$ cells within young MB- and LB-HSC and aged MB- and LB-HSC (n = 3/group, t test).

(G) At left, representative histogram of p-EGFR (Y1173) levels in BM 34$^-$KSL cells from young mice at 15 min of treatment with 20 ng/mL EGF or media alone; at right, MFI of p-EGFR levels in each group (n = 9/group, t test).

(H) At left, representative histogram of p-EGFR (Y1173) levels in BM 34$^-$KSL cells from aged mice at 15 min of treatment with 100 ng/mL EGF or media alone; at right, MFI of p-EGFR levels in BM 34$^-$KSL cells from each group (n = 8/group, t test). Data are represented as means +/− SEM. *p < 0.05, **p < 0.01, ***p < 0.001.

suppression of CFU-GM generation, with increased multilineage CFU-granulocyte erythroid megakaryocyte monocyte (CFU-GEMM) generation (Figure 2H). Treatment with NU7441, a specific DNA-PKcs inhibitor,[34] blocked this effect of EGF on aged HSCs, suggesting that DNA PK-cs is important for EGF-mediated reestablishment of multilineage differentiation in aged HSCs. Separately, treatment with the Akt-inhibitor, MK2206,[34] also blocked EGF-mediated reestablishment of multilineage colony forming capacity in aged HSCs, suggesting that Akt activation was also required for this effect (Figure 2I).

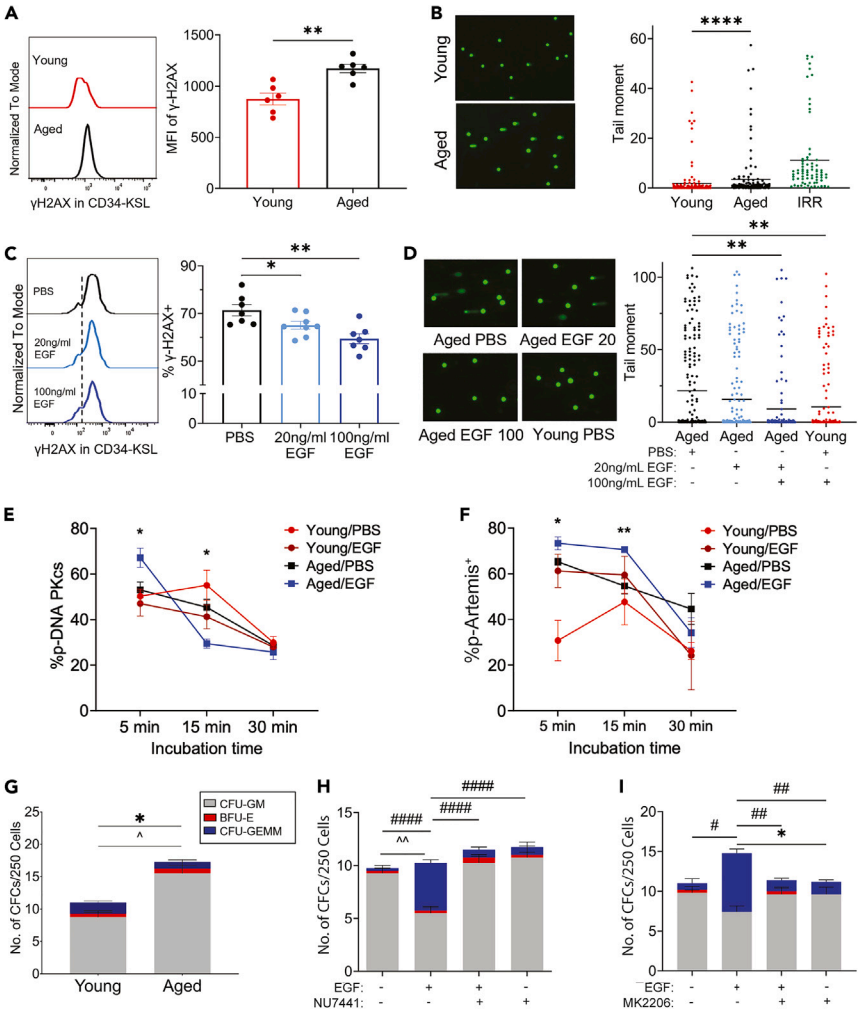

Figure 2. EGF treatment promotes NHEJ DNA repair in aged HSCs

(A) At left, representative histograms show the levels of γ-H2AX in young and aged BM 34$^-$KSL cells; at right, MFI of γ-H2AX is shown in each population (n = 6/group, t test).

(B) Representative Comet assay shows tail moment length in BM 34$^-$KSL cells from young and aged mice; at right, mean tail moment lengths in both populations and in irradiated (IRR = 200 cGy) control sample (young, n = 171, aged, n = 142, IRR = 72, ANOVA).

(C) Representative histograms show γ-H2AX levels in aged BM 34$^-$KSL cells cultured in TSF media alone or TSF media + EGF for 2 h; at right, mean levels of γ-H2AX in aged BM 34$^-$KSL cells in culture (n = 7–8/group, ANOVA).

(D) At left, representative Comet assay of aged BM 34$^-$KSL cells from each culture condition at 1 h and young BM 34$^-$KSL control cells; at right, mean tail moment lengths in each condition shown (aged/TSF, n = 190, aged/20 ng/mL EGF, n = 169, aged/100 ng/mL EGF, n = 132, young/TSF, n = 168, ANOVA).

(E) Mean %p-DNA-PK-cs$^+$ BM KSL cells from aged and young mice at 5 min, 15 min, and 30 min of culture in serum-starved IMDM +/− EGF (n = 3/group, t test).

(F) Mean %p-Artemis$^+$ BM KSL cells at 5 min, 15 min, and 30 min of culture +/− EGF (n = 3/group, t test).

(G) Mean numbers of CFCs from BM 34$^-$KSL cells (250 per dish) from young and aged mice (n = 4/group, *p < 0.05 for total CFCs, ^p < 0.05 for CFU-GM).

(H) At left, total numbers of CFCs from aged BM 34$^-$KSL cells cultured × 7 days with TSF media alone +/− EGF and +/− DNA PK-cs inhibitor, NU7441; at right, numbers of CFU-GEMMs per each condition (n = 4/group, ^^p < 0.01 for CFU-GM, ####p < 0.0001 for CFU-GEMMs).

(I) Total CFCs (left) and CFU-GEMMs (right) from aged BM 34-KSL cells cultured × 7 days with TSF media alone +/− EGF and +/− Akt inhibitor, MK2206 (n = 5/group, *p < 0.05 for total CFCs, #p < 0.05 and ##p < 0.01 for CFU-GEMMs). Data are represented as means +/− SEM. *p < 0.05, **p < 0.01, ***p < 0.001, ****p < 0.0001.

EGF treatment *in vitro* increases the repopulating capacity of aged HSCs

In order to determine if EGF treatment could rejuvenate the function of aged HSCs, we isolated BM 34$^-$KSL cells from aged and young mice and cultured for 7 days in media with or without 100 ng/mL EGF. Treatment with EGF modestly decreased total cell expansion and %KSL cells in culture compared to TSF media alone (Figure 3A). However, EGF-treated aged HSCs displayed 2-fold increased percentages of CD150$^+$CD48$^-$KSL (SLAM KSL) HSCs compared to aged HSCs cultured with media alone (Figure 3A). In order to determine if EGF treatment

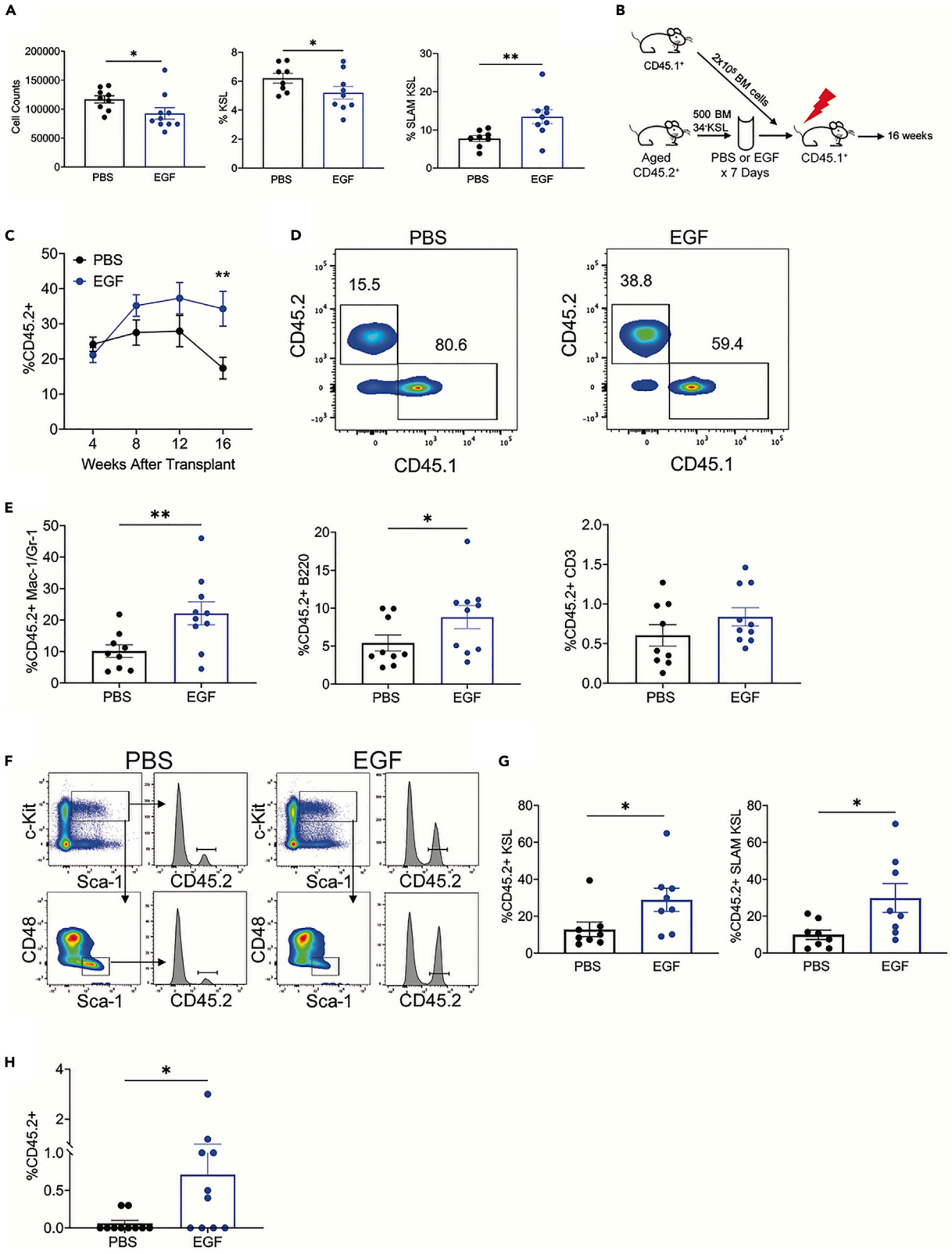
A
Cell Counts
% KSL
% SLAM KSL
PBS
EGF
B
CD45.1+
2x10⁵ BM cells
500 BM 34-KSL
Aged CD45.2+
PBS or EGF x 7 Days
CD45.1+
16 weeks
C
PBS
EGF
%CD45.2+
Weeks After Transplant
D
PBS
EGF
CD45.2
CD45.1
15.5
80.6
38.8
59.4
E
%CD45.2+ Mac-1/Gr-1
%CD45.2+ B220
%CD45.2+ CD3
F
PBS
EGF
c-Kit
Sca-1
CD48
CD45.2
G
%CD45.2+ KSL
%CD45.2+ SLAM KSL
H
%CD45.2+

Figure 3. EGF treatment *in vitro* improves the competitive repopulating capacity of aged HSCs

(A) Total cell counts, %KSL cells and % SLAM KSL cells at day +7 of culture of aged BM 34$^-$KSL cells with Media alone (TSF) or media + EGF (n = 9–10/group, t test).

(B) Schematic representation of the competitive transplantation assays performed. Recipient mice irradiated with 875 cGy TBI.

(C) Donor CD45.2+ cell engraftment over time in the PB of primary recipient CD45.1+ mice transplanted competitively with the progeny of 500 aged BM 34-KSL cells cultured with media alone or media + EGF x 7 days (n = 9-10/group). (D) Representative flow cytometric analysis of donor CD45.2$^+$ cell engraftment in the PB of CD45.1$^+$ recipient mice at 16 weeks following transplantation as described in (C).

(E) Mean percentages of donor CD45.2$^+$, CD45.2$^+$Mac-1/Gr-1$^+$ cells, CD45.2$^+$B220$^+$ cells, and CD45.2$^+$CD3$^+$ cells in the PB of CD45.1$^+$ recipient mice at 16 weeks post competitive transplantation of the progeny of 500 aged BM 34$^-$KSL cells treated with media alone or media + EGF (*n* = 9–10/group, ANOVA).

(F) Representative flow cytometric analysis of donor CD45.2$^+$ cell engraftment within the BM KSL population and within BM CD150$^+$CD48$^-$KSL HSCs at week 16 in recipient mice transplanted with the progeny of aged BM 34$^-$KSL cells treated with media alone or media + EGF.

(G) Mean %CD45.2$^+$KSL cells and %CD45.2$^+$CD150$^+$CD48$^-$KSL (SLAM KSL) cells in recipient mice transplanted with the progeny of culture with media alone or media + EGF (*n* = 9/group, t test).

(H) Mean percentages of donor CD45.2$^+$ cells in the PB of secondary mice that were transplanted with 1 × 10^6 BM cells collected at 16 weeks from primary recipient mice that were competitively transplanted with the progeny of aged BM 34$^-$KSL cells cultured × 7 days with media alone or media + EGF (*n* = 9/group, t test). Data are represented as means +/− SEM. **p* < 0.05, ***p* < 0.01, ****p* < 0.001.

affected HSC self-renewal capacity, we performed competitive transplantation assays of aged BM HSCs (CD45.2$^+$) treated with media + EGF or Media alone × 7 days (Figure 3B). A time course analysis of donor CD45.2$^+$ cell engraftment in the peripheral blood (PB) of recipient CD45.1$^+$ mice transplanted competitively with the progeny of 5 × 10^2 BM 34$^-$KSL cells cultured with EGF or saline revealed increasing engraftment over time in the EGF group with significantly increased donor CD45.2$^+$ engraftment at 16 weeks (Figure 3C). Representative total donor CD45.2$^+$ cell engraftment in the PB of recipient mice at 16 weeks is shown in Figure 3D. Donor CD45.2$^+$ cell contribution to the BM Mac1/Gr1$^+$ myeloid lineage and B220$^+$ B cell lineage was also increased in mice transplanted with EGF-cultured, aged HSCs (Figure 3E). Analysis of donor cell engraftment within the BM SLAM KSL HSC and KSL progenitor populations also revealed increased donor CD45.2$^+$ cell engraftment within both populations in mice transplanted with EGF-treated, aged HSCs compared to mice transplanted with aged HSCs treated with media alone (Figures 3F and 3G). Secondary transplants were performed in which CD45.1$^+$ mice were transplanted with 1 × 10^6 BM cells collected at 16 weeks from primary recipient mice previously transplanted with the progeny of 1 × 10^3 aged BM 34$^-$KSL cells cultured × 7 days with or without EGF. While donor CD45.1$^+$ engraftment was low in both groups, mice in the aged, EGF-treatment group displayed significantly increased donor engraftment at 16 weeks in secondary mice compared to aged, control mice (Figure 3H). These data suggest that short-term treatment with EGF increased the long-term repopulating capacity of aged HSCs.

We also measured the effect of EGF treatment on BM 34$^-$KSL cells from young mice (8–12 weeks). EGF treatment ×7 days caused no change in total cell expansion but caused a decrease in %KSL cells and an increase in %SLAM KSL cells compared to culture with TSF media alone (Figure S3A). EGF treatment did not affect CFC production from young BM 34$^-$KSL cells in culture compared to media alone and competitive transplantation assays demonstrated no difference in donor CD45.2$^+$ cell engraftment at 16 weeks post-transplant in lethally irradiated CD45.1$^+$ recipient mice between the BM 34$^-$KSL cells cultured with media + EGF versus cells cultures with media alone (Figures S3B–S3D). No significant differences were observed in donor CD45.2$^+$ cell engraftment within BM KSL or SLAM KSL LT-HSC populations between the 2 groups (Figures S3E and S3F). These data suggest that EGF treatment produced specific effects on aged HSCs that were not detected in young HSCs.

Systemic administration of EGF improves HSC self-renewal capacity in aged mice

We next tested whether systemic administration of EGF to aged mice could rejuvenate HSC function *in vivo*. We administered 1 μg/g EGF or saline intraperitoneally (IP) every other day for six weeks to aged *C57BL/6* mice (Figure 4A). In preliminary studies, we observed that systemic administration of 10 μg or 20 μg EGF to adult C57BL/6 mice yielded a significant increase in EGF levels in the PB serum and BM of mice at +1 and +6 h post-administration (Figures S4A and S4B). In control mice treated with PBS alone, aged mice displayed increased percentages of Mac-1/Gr-1$^+$ PB cells compared to young mice, consistent with the myeloid skewing described with aging (Figure 4B).[36,44] Aged mice treated × 6 weeks with EGF demonstrated correction in percentages of Mac-1/Gr-1$^+$ PB cells to be comparable to that of young mice (Figure 4B), without correction of percentages of B cells or T cells, or BM KSL cells (Figures 4C–4E). Of note, in a complementary study, we administered 1 μg/g EGF or PBS subcutaneously daily × 21 days to aged C57BL/6 mice. Mice treated with EGF displayed significantly decreased percentages of PB Mac-1/Gr-1$^+$ cells and increased percentages of PB B and T cells, but the latter did not reach statistical significance (Figure S4C). We detected no differences in BM cell counts, but EGF-treated mice demonstrated significantly reduced BM colony forming cells (total), decreased BM CFU-GMs and increased multipotent CFU-GEMMs compared to PBS-treated controls (Figures S4D and S4E). No differences were detected in percentages of BM KSL cells, SLAM KSL HSCs, or CD229- SLAM KSL cells (MB-HSCs)(Figure S4F).

In order to assess the effect of systemic administration of EGF on HSC repopulating capacity in aged mice, we transplanted equal doses of BM cells (3 × 10^4) from aged donor CD45.2$^+$ mice treated × 6 weeks with EGF or saline into recipient CD45.1$^+$ mice, along with 2 × 10^5 CD45.1$^+$ BM competitor cells, and compared donor hematopoietic cell engraftment over time. Mice transplanted with BM cells from aged mice treated with EGF displayed significantly increased donor cell engraftment in the PB at 16 weeks post-transplant compared to recipients of BM cells from aged mice treated with saline (Figure 4F). Competitive secondary transplants demonstrated exhaustion of long-term HSC repopulating capacity in recipients of BM from aged control mice, whereas recipients of BM cells from aged mice treated with EGF demonstrated sustained engraftment through 16 weeks (Figure 4F). Donor cell engraftment in the BM KSL population was increased

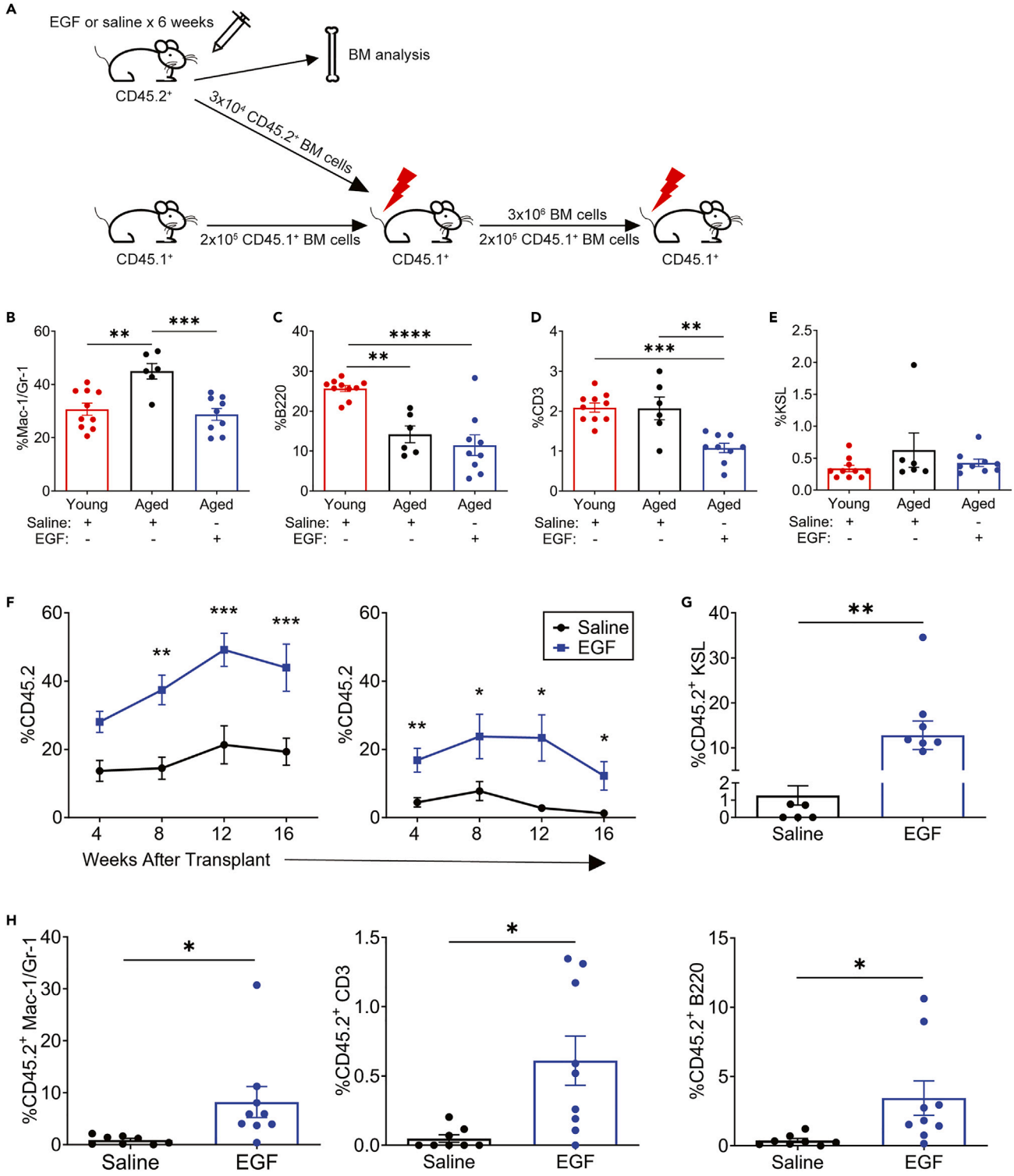

Figure 4. Systemic administration of EGF increases the repopulating capacity of BM HSCs in aged mice

(A) Schema of *in vivo* administration of EGF or saline intraperitoneally (IP) every other day for 6 weeks in young and aged CD45.2$^+$ mice, followed by primary and secondary competitive transplantation assays.

(B) Percentages of BM myeloid cells, (C) B cells, and (D) T cells in C57BL/6 mice following treatment with EGF or saline x 6 weeks (n = 10 young/saline, n = 6 aged/saline, n = 9 aged/EGF, 1-way ANOVA).

Figure 4. *Continued*

(E) Percentages of BM KSL cells in mice following EGF or saline treatment (n = 10 young/saline, n = 6 aged/saline, n = 9 aged/EGF, 1-way ANOVA).

(F) At left, percentages of donor CD45.2$^+$ cells in the PB of CD45.1$^+$ recipient mice over time following transplantation of BM cells from aged, saline-treated mice or aged, EGF treated mice (n = 12 aged + saline, n = 10 aged + EGF, two-way ANOVA); at right, CD45.2$^+$ cell engraftment in the PB of secondary, competitively transplanted CD45.1$^+$ mice is shown over time (n = 8 aged + saline, n = 9 aged + EGF, two-way ANOVA).

(G) Percentages of BM CD45.2$^+$ KSL cells at 16 weeks in secondary transplanted mice (n = 5–7/group, t test).

(H) Percentages of CD45.2$^+$ myeloid, B cell, and T cell chimerism in the BM of secondary transplanted mice at 16 weeks (n = 8 aged+saline, n = 9 aged+EGF, one-way ANOVA). Data represented as means +/− SEM. *p < 0.05, **p < 0.01, ***p < 0.001, ****p < 0.0001.

(Figure 4G) and donor myeloid, B cell, and T cell chimerism were all increased in secondary transplanted mice in the EGF treatment group, suggesting that systemic treatment with EGF rescued LT-HSC repopulating capacity in aged mice (Figure 4H).

EGF shifts the transcriptional program of aged HSCs to HSC self-renewal program

Since EGF treatment improved the repopulating capacity of aged HSCs, we measured the effects of EGF treatment on the transcriptional profile of aged HSCs. For this analysis, young and aged C57BL/6 mice were treated x 72 h with EGF or saline subcutaneously daily and BM 34$^-$KSL HSCs were isolated by fluorescence-activated cell sorting (FACS) for single-cell RNA sequence analysis (scRNA-seq), as previously described (Figures 5A and S5A).[45] After cell sorting, we subjected 1 × 10^3 BM 34$^-$KSL cells in each condition to scRNA-seq using the 10x Genomics platform (see STAR Methods). This analysis revealed 4 major clusters of HSCs based on shifts in transcriptional profile, as shown in the uniform manifold and approximation projection (UMAP) space plot (Figure 5B). Based on gene ontology (GO) term pathway enrichment analysis, we assigned the following labels to each major HSC cluster, following methods described by Fast et al.[45]: cluster 0 = hematopoietic development and function, cluster 1 = cell death and survival, cluster 2 = hematologic disease, and cluster 3 = organismal injury (Figure 6B). We also identified 3 smaller clusters with gene enrichment in immune response (cluster 4), morphology (cluster 5), and immunological disease (cluster 6). BM 34$^-$KSL cells from young mice showed the highest density in cluster 0, hematopoietic development and function (Figure 6C). Conversely, HSCs from aged mice displayed a shift in transcription into cluster 1, cell death and survival, compared to young HSCs (Figure 5C). However, BM 34$^-$KSL HSCs from aged mice treated x 72 h with EGF shifted gene enrichment primarily back to cluster 0, hematopoietic development and function. Ingenuity pathway analysis (IPA) of the transcripts represented in aged HSCs treated with EGF revealed enrichment for genes associated with hematologic system development and function, cellular development, immune response, and hematopoiesis, whereas aged HSCs from mice treated with PBS displayed enrichment for expression of genes involved in cell death and survival, organismal injury, connective tissue function, and tissue morphology (Figures S5B and S5C). A heatmap of gene expression of aged, EGF-treated HSCs revealed upregulation of genes required for HSC self-renewal, such as early growth response gene 1 (*Egr1*)[46,47] and phosphatase and tensin homolog (*Pten*),[48] genes that regulate hematopoietic function, such as inositol polyphosphate-5-phosphatase D (*Inpp5d*), which encodes SHIP1,[49] and IKAROS family zinc finger 1 (*Ikzf1*), which encodes Ikaros,[50] Pecam1,[51] which is expressed during hematopoietic specification of embryonic stem cells, and *Adgrg3*, which encodes the G protein coupled receptor, GPR97,[52] and regulates HSC development during embryogenesis (Figure 5D). While the scRNA-seq analysis does not discriminate whether EGF stimulates a small subset of undamaged HSCs, competitively fills gaps left by damaged HSCs or reverses the vitality of aged HSCs, the results suggest that EGF treatment shifts the transcriptional program of HSCs in aged mice toward that of hematopoietic identity and function.

We also examined the effect of EGF treatment on the expression of genes whose expression has been linked to aging across multiple tissues[53] and genes associated with DNA repair mechanisms (Figures 5E and 5F). EGF treatment was associated with up- and down-regulation of expression of genes involved in aging processes, including *Tmsb10*, which encodes thymosin B-10, an actin sequestering protein,[54] *Lars2*, which encodes leucyl tRNA synthetase 2,[55] and *Cdc42*, a RhoGTPase that regulates HSC polarity and aging.[56] EGF treatment was associated with more uniform effects on the expression of DNA repair genes, including increased expression of *Pkrdc*, which encodes DNA PK-cs, *Xrcc6*, which encodes Ku70 component of the NHEJ complex,[34,39] *Babam2*, an anti-apoptotic molecule which is part of the BRCA-1A DNA repair complex,[57] and *Smarcb1*, which is implicated in DNA double-strand repair and homologous recombination.[58]

Since the scRNA-seq analysis suggested that systemic EGF administration increased expression of *Egr1*, and its target gene, *Pten*, in aged HSCs (Figures 5G and 5H), and both genes are implicated in control of HSC self-renewal,[47,48] we confirmed by RT-qPCR that EGF treatment increased Egr1 expression in aged BM 34$^-$KSL HSCs (Figure 5I). Of note, EGF treatment had no effect on Egr1 expression in young HSCs (Figure S5D). In order to determine whether Egr1 was required for EGF-mediated effects of HSC colony formation, we transduced aged BM 34$^-$KSL cells with a lentiviral shRNA targeting Egr1 or shRNA-control. Treatment of aged BM 34$^-$KSL cells with shRNA-Egr1 caused >80% loss of BM 34$^-$KSL cells in culture, so we instead evaluated whether inhibition of PTEN, which is transcriptionally regulated by Egr1,[59] could abrogate EGF effects on HSC colony forming cells. Treatment of aged BM 34$^-$KSL cells with VO-OHpic trihydrate, a selective inhibitor of PTEN,[60] inhibited EGF effects on CFU-GEMM generation and suppression of myeloid differentiation (Figure 5J). Of note, VO-OHpic trihydrate had no effect on CFC generation from young HSCs treated with or without EGF (Figure S5E). These data suggest that EGF modulation of differentiation in aged HSCs may be dependent on PTEN.

EGFR silencing in hematopoietic cells decreases HSC repopulating capacity in aging

In order to determine if EGFR signaling is required for the maintenance of hematopoiesis during aging, we utilized the *SCL-tTA;EGFR-DN* transgenic mouse model,[34] in which expression of a dominant negative EGFR, containing a truncated cytoplasmic tyrosine kinase

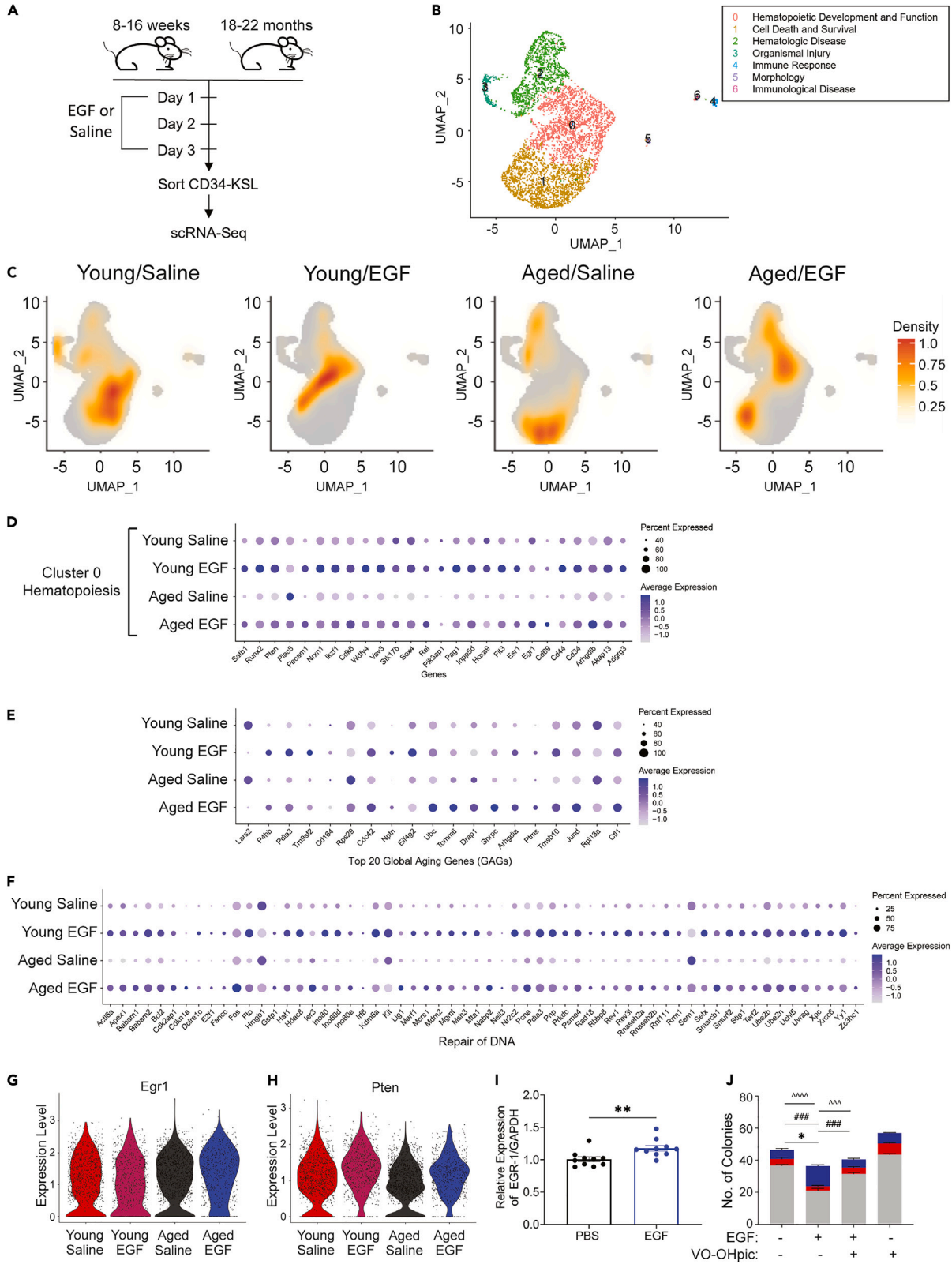
A
8-16 weeks
18-22 months
EGF or Saline
Day 1
Day 2
Day 3
Sort CD34-KSL
scRNA-Seq
B
0 Hematopoietic Development and Function
1 Cell Death and Survival
2 Hematologic Disease
3 Organismal Injury
4 Immune Response
5 Morphology
6 Immunological Disease
UMAP_1
UMAP_2
C
Young/Saline
Young/EGF
Aged/Saline
Aged/EGF
Density
D
Cluster 0 Hematopoiesis
Young Saline
Young EGF
Aged Saline
Aged EGF
Percent Expressed
Average Expression
Genes
E
Top 20 Global Aging Genes (GAGs)
F
Repair of DNA
G
Egr1
Expression Level
H
Pten
I
Relative Expression of EGR-1/GAPDH
PBS
EGF
J
No. of Colonies
EGF:
VO-OHpic:

Figure 5. EGF drives a hematopoiesis transcriptional program in aged HSCs

(A) Schematic representation of systemic administration of EGF or saline to young and aged C57Bl/6 mice daily × 3 days, followed by isolation of BM 34$^-$KSL cells for single cell RNA sequence analysis.

(B) Uniform manifold approximation and projection (UMAP) plot of BM 34$^-$KSL cell clusters (n = 1,693) with labels assigned to each HSC cluster based on gene ontology term pathway enrichment analysis.

(C) UMAP density graphs of BM CD34$^-$KSL distribution for each of the 4 experimental groups.

(D) Dot plots of expression level and percent expression of hematopoiesis genes in BM 34$^-$KSL cells from the treatment groups shown. Size of dot indicates the numbers of cells that express the gene and the color indicates the expression level.

(E) Dot plots of average and percent expression of aging associated genes in the groups shown.

(F) Dot plots of average and percent expression of DNA repair genes in the groups shown.

(G) Violin plots showing expression of Egr1 from single cell RNA-seq analysis of HSCs from young and aged mice treated with EGF or saline.

(H) Violin plots of Pten expression in HSCs from young and aged mice treated with EGF or saline.

(I) Expression of Egr1 in aged BM 34$^-$KSL cells cultured for 48 h with EGF or PBS (n = 10/group, t test).

(J) Mean numbers of CFCs in BM 34$^-$KSL cells cultured × 72 h with media alone, media + EGF, Media + EGF + VO-OHpic, or media + VO-OHpic alone (n = 4 replicates per group, 250 cells/dish, *p < 0.05 for total CFCs, ^^^p < 0.001 for CFU-GMs, ###p < 0.001 for CFU-GEMMs). Data represented as means +/− SEM.

domain-form of EGFR (EGFR-DN), is under control of doxycycline (dox-off system) specifically within cells expressing the stem cell leukemia (*Scl/Tal1*) gene, which are restricted to the hematopoietic cell compartment (Figure 6A).[34,61–63] *EGFR-DN* expression in *Scl*-expressing cells disrupts the activation of EGFR signaling in HSPCs via expression of the dominant-negative EGFR (Figure S6A).[34] BM KSL cells from EGFR wild-type (EGFR WT) mice displayed increased p-EGFR in response to EGF treatment, whereas BM KSL cells from EGFR DN mice demonstrated no increase in p-EGFR (Figure S6B).

EGFR-DN mice displayed no differences in PB white blood cell counts (WBC), hemoglobin, or platelet counts compared to EGFR WT mice (Figure S6C) but did demonstrate increased percentages of PB neutrophils and decreased lymphocytes (Figure 6B). *EGFR-DN* mice also displayed increased percentages of BM KSL cells (Figures 6C and 6D) and increased BM myeloid skewing (Figure 6E), without significant changes in percentages of B and T cells (Figure 6E). *EGFR-DN* mice also displayed no significant differences in percentages of BM CD229$^-$ MB-HSCs (Figure S6D) but demonstrated decreased BM CFC content compared to *EGFR-WT* mice (Figure 6F).

BM cells from *EGFR-DN* mice displayed decreased radioprotective capacity compared to BM cells from *EGFR-WT* mice, as measured by limiting dose BM transplantation (1 × 10^5 cells) into lethally irradiated F1 progeny recipient mice (Figure 6G). Congenic mice (CD45.1$^+$) transplanted competitively with BM cells from *EGFR-DN* mice displayed decreased primary and secondary engraftment of donor CD45.2$^+$ hematopoietic cells in the PB over time compared to mice transplanted with the identical dose of BM cells from *EGFR-WT* mice (Figures 6H–6J and S6E). These results suggest that the loss of EGFR signaling causes a decrease in HSC function in middle aged mice.

BM 34$^-$KSL cells from *EGFR DN* mice displayed a modest decrease in MFI of γ-H2AX compared to 34$^-$KSL cells from *EGFR WT* mice (Figure S7A), and no differences in %SA-β-galactosidase$^+$ KSL or mitochondrial superoxide (mitoSOX)$^+$ KSL cells were observed (Figures S7B and S7C). Bulk RNA-seq analysis of BM 34$^-$KSL HSCs from *EGFR DN* mice and *EGFR WT* mice did not reveal patterns of differential gene expression in hematopoiesis genes (Figure S7D), aging genes (Figure S7E) or DNA repair genes (Figure S7F), possibly reflecting transcriptional compensation for loss of EGFR signaling in hematopoietic cells in the transgenic mouse model.

DISCUSSION

During aging, HSCs increase in frequency, become myeloid-biased with diminished lymphoid potential, and lose multilineage self-renewal capacity.[12,64] Simultaneously, clonal expansion occurs and risk for transformation to myelodysplastic disorders and leukemia increases.[64] Several studies have suggested that HSC aging is largely a cell-autonomous process, presaged by molecular deterioration of the HSC pool.[36,65,66] In keeping with this hypothesis, Ho et al. demonstrated that transplantation of aged HSCs into young mice or treatment of aged HSCs with bloodborne factors from young mice could not restore the function of aged HSCs, suggesting that extrinsic signaling was unlikely to reverse the HSC aging process.[28] Here, we have shown that *in vitro* or *in vivo* treatment with EGF augments the repopulating capacity of aged HSCs while suppressing myeloid bias. Our data suggest that EGF-driven reestablishment of multipotency is mediated, at least in part, through activation of DNA-PKcs. This may be explained by non-canonical functions of DNA-PKcs in regulating transcription. For example, DNA-PKcs phosphorylates the transcription factor, Egr1, thereby augmenting its transcription factor activity.[67] Egr1 and its target gene, Pten, have essential functions in maintaining long-term HSC self-renewal capacity.[46–48] Here, we demonstrated that inhibition of PTEN blocked EGF-mediated suppression of HSC myeloid differentiation and induction of multipotent progenitor production. These results suggest further studies are warranted to characterize the role of Egr1 and PTEN in mediating EGF effects on the self-renewal capacity of aged HSCs. EGF treatment also caused rapid upregulation in expression of several DNA repair genes in aged HSCs; in future studies, we will explore the functional role of these specific DNA repair genes in mediating EGF effects on aging HSCs.

We also discovered here that EGFR surface expression is increased on aged HSCs, commensurate with increased EGF levels in the BM of aged mice, and that EGFR expression is increased on myeloid biased HSCs relative to lymphoid biased HSCs. Concordantly, EGFR expression enriches for myeloid biased HSCs in aged mice. These results suggest the possibility that EGFR signaling may regulate the HSC shift between myeloid and lymphoid predilection that occurs with aging. Ross et al.[68] recently demonstrated that antibody-based depletion of myeloid biased HSCs restored functional characteristics of a youthful immune system to aged mice. We will pursue studies going forward to determine whether modulation of EGFR signaling can alter the propensity of aging HSCs toward myeloid bias and immune dysfunction.

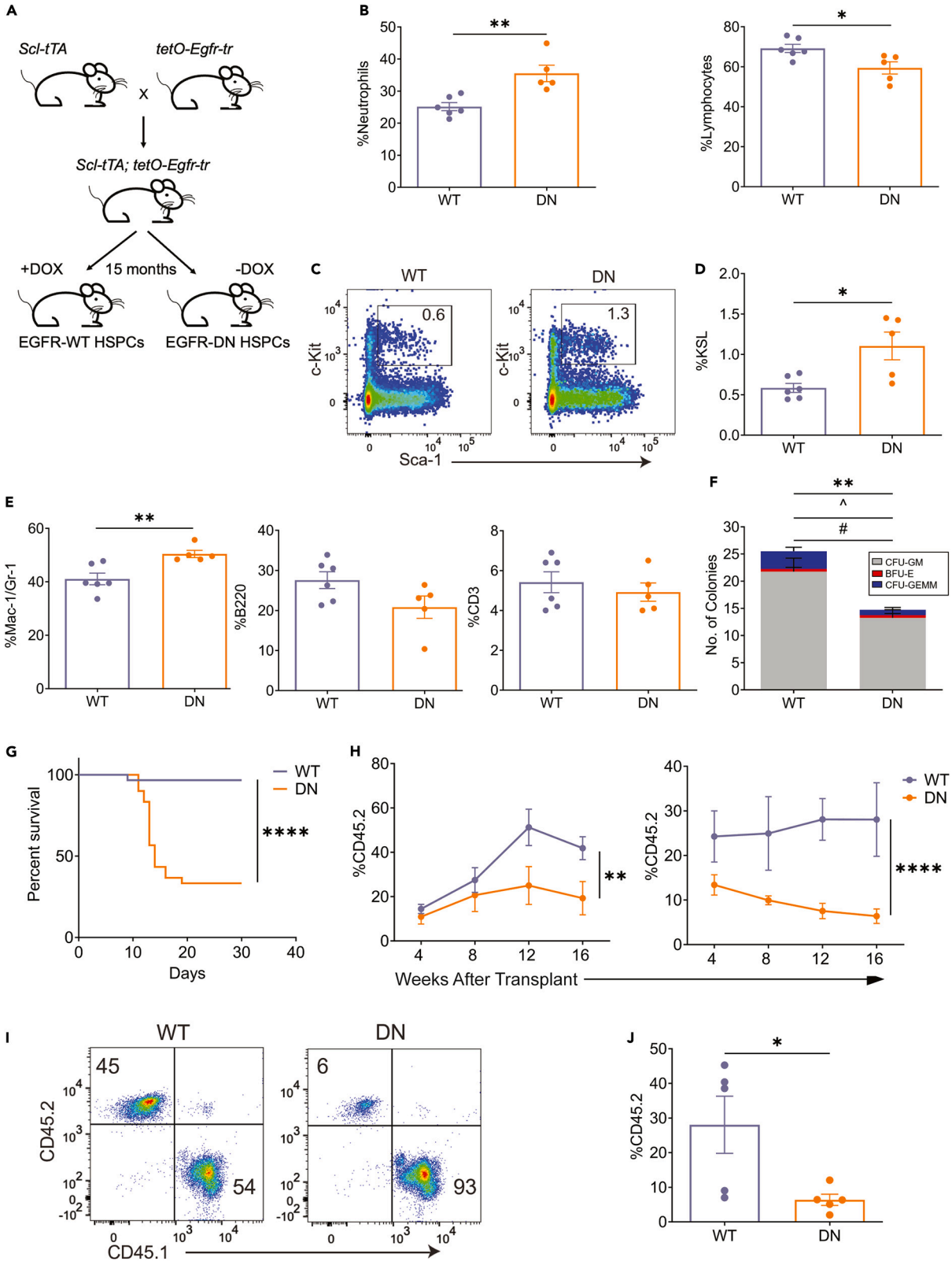
A
Scl-tTA
tetO-Egfr-tr
X
Scl-tTA; tetO-Egfr-tr
+DOX
15 months
-DOX
EGFR-WT HSPCs
EGFR-DN HSPCs
B
%Neutrophils
**
WT
DN
%Lymphocytes
*
C
WT
DN
0.6
1.3
c-Kit
Sca-1
D
%KSL
E
%Mac-1/Gr-1
%B220
%CD3
F
No. of Colonies
CFU-GM
BFU-E
CFU-GEMM
G
Percent survival
Days
****
H
%CD45.2
Weeks After Transplant
I
45
54
6
93
CD45.2
CD45.1
J

Figure 6. Deletion of EGFR in HSPCs accelerates hematopoietic aging

(A) Transgenic model in which expression of a dominant negative EGFR (EGFR-DN) is under control of doxycycline (DOX off) within *Scl*-expressing hematopoietic cells; mice were treated with or without DOX (+/− DOX) × 12–15 months before analysis.

(B) Percentages of PB neutrophils and lymphocytes in EGFR-DN (DN) and EGFR-WT (WT) mice (n = 6 WT, n = 5 DN, two-tailed t test).

(C) Representative flow cytometric analysis of BM KSL cells in WT and DN mice.

(D) Percentages of BM KSL cells (n = 6 WT, n = 5 DN, two-tailed t test) and (E) Percentages of BM myeloid cells, B cells, and T cells in WT and DN mice (n = 6 WT, n = 5 DN, two-tailed t test).

(F) Numbers of BM CFCs in WT and DN mice (n = 6/group, two-way ANOVA).

(G) Percent survival of adult *C57BL/6* mice following 1,175 cGy TBI and infusion of 1×10^4 BM cells from WT or DN mice (n = 20/group, log rank/Mantel-Cox test).

(H) At left, percentages of $CD45.2^+$ donor cells in the PB of primary recipient $CD45.1^+$ mice over time following competitive transplantation of 3×10^4 $CD45.2^+$ BM cells from WT and DN mice (n = 8 WT, n = 10 DN, two-way ANOVA); at right, $CD45.2^+$ cell engraftment in secondary mice over time following transplantation with 3×10^6 BM cells collected at 16 weeks from primary recipient mice (n = 5 WT, n = 5 DN, two-way ANOVA).

(I) Representative flow cytometric analysis of $CD45.2^+$ cell engraftment in the PB at 16 weeks in secondary $CD45.1^+$ mice transplanted with BM cells from primary recipients in the WT or DN group.

(J) $CD45.2^+$ cell engraftment in the PB at 16 weeks in secondary transplanted $CD45.1^+$ mice (n = 5 WT, n = 5 DN, one-way ANOVA). Data represented as means +/− SEM. *$p \leq 0.05$, **$p \leq 0.01$, ****$p \leq 0.0001$.

While our studies suggest that EGF treatment can improve the repopulating capacity of aged HSCs and that EGFR signaling has an important role in maintaining HSC repopulating capacity during aging, we did not observe significant effects of EGF or EGFR signaling on other characteristics of aging, such as HSC senescence, reactive oxygen species (ROS) accumulation or the expression of aging-associated genes. These results suggest, perhaps surprisingly, that self-renewal capacity of aged HSCs may be more amenable to extrinsically driven augmentation than other aging processes. Our findings are also consistent with the recent study by Mitchell et al.[24] who demonstrated that blockade of IL-1β, produced by the proinflammatory aged endosteal niche, was able to improve HSC repopulating capacity *in vivo*.

Limitations of the study

We showed here that EGF treatment decreased DNA damage and augmented DNA PK-cs activity in aged HSCs, but we did not determine whether EGF-mediated effects on aged HSC self-renewal were dependent on augmentation of DNA repair. Our transplantation assays utilized whole BM cells from EGF-treated and EGFR-deficient mice, rather than purified HSCs, so our studies do not exclude the possibility that EGF-EGFR signaling regulates the repopulating capacity of aged HSCs indirectly via other BM cell populations or niche effects. While we observed that EGF treatment and EGFR deletion altered the repopulating capacity of aged HSCs, we detected no effects of EGF-EGFR signaling on HSC senescence, ROS generation, or aging-associated processes.

STAR★METHODS

Detailed methods are provided in the online version of this paper and include the following:

- KEY RESOURCES TABLE
- RESOURCE AVAILABILITY
  - Lead contact
  - Materials availability
  - Data and code availability
- EXPERIMENTAL MODEL AND STUDY PARTICIPANT DETAILS
  - Mice
  - Cell culture
- METHOD DETAILS
  - Competitive repopulation assay
  - Single cell RNA sequencing
  - ELISA of EGF receptor ligands
  - Flow cytometric analyses and cell sorting
  - qRTPCR
  - Comet assay
  - Cell cycle and apoptosis assays
  - CFC assay
  - Transplantation assays
  - Immunofluorescence microscopy for γ-H2AX
  - Bulk RNAseq
  - SA-β-Galactosidase assay
  - Mitochondrial superoxide (MitoSOX) assay
- QUANTIFICATION AND STATISTICAL ANALYSIS

SUPPLEMENTAL INFORMATION

Supplemental information can be found online at https://doi.org/10.1016/j.isci.2024.110306.

ACKNOWLEDGMENTS

We thank Kevin Tang, Lisa C. Valicente, and Natalia Kozlova for assistance with DNA damage assays. We thank Edo Israely from the Cedars Sinai flow cytometry core facility for assistance with cell sorting and Sarah Song from the Cedars Sinai Applied Genomics, Computation and Translational Core; we thank Jeffrey Calimlim, Felicia Codrea, and Jessica Scholes from the Broad Stem Cell Research Center FACS Core Facility for help with sorting. We thank Liman Zhao for animal colony management and Christina M. Termini for scientific consultation. This work was supported in part by funding from the National Heart, Lung, and Blood Institute (NHLBI) grant R01 HL-086998 (J.P.C.) and National Institute of Allergy and Infectious Diseases (NIAID) grant AI156922 (J.P.C.). V.Y.C. is supported by NIH K08HL138305.

AUTHOR CONTRIBUTIONS

J.P.C. and V.Y.C. designed the study, and J.P.C. directed the study; V.Y.C., Y.H., S.G., M.B., A.C., R.S.K., T.F., A.P., K.P., E.T., M.L., J.K., Y.Z., J.J.L., J.P.S., H.A.H., and P.Y. performed the experiments; V.Y.C. and J.P.C. wrote the paper, with input from the other authors.

DECLARATION OF INTERESTS

The authors declare no competing interests.

Received: December 21, 2023
Revised: February 19, 2024
Accepted: June 17, 2024
Published: June 19, 2024

REFERENCES

1. Morrison, S.J., Wandycz, A.M., Akashi, K., Globerson, A., and Weissman, I.L. (1996). The aging of hematopoietic stem cells. Nat. Med. *2*, 1011–1016.
2. de Haan, G., Nijhof, W., and Van Zant, G. (1997). Mouse strain-dependent changes in frequency and proliferation of hematopoietic stem cells during aging: correlation between lifespan and cycling activity. Blood *89*, 1543–1550.
3. Sudo, K., Ema, H., Morita, Y., and Nakauchi, H. (2000). Age-associated characteristics of murine hematopoietic stem cells. J. Exp. Med. *192*, 1273–1280.
4. SEER Program (National Cancer Institute (U.S.)), National Center for Health Statistics (U.S.), National Cancer Institute (U.S.). Surveillance Program., National Cancer Institute (U.S.). Cancer Statistics Branch., and National Cancer Institute (U.S.). Cancer Control Research Program (1993). SEER Cancer Statistics Review (NIH publication. U.S. Dept. of Health and Human Services, Public Health Service, National Institutes of Health, National Cancer Institute).
5. Forman, D., Stockton, D., Møller, H., Quinn, M., Babb, P., De Angelis, R., and Micheli, A. (2003). Cancer prevalence in the UK: results from the EUROPREVAL study. Ann. Oncol. *14*, 648–654. https://doi.org/10.1093/annonc/mdg169.
6. McElhaney, J.E., and Dutz, J.P. (2008). Better influenza vaccines for older people: what will it take? J. Infect. Dis. *198*, 632–634. https://doi.org/10.1086/590435.
7. Fleming, D.M., and Elliot, A.J. (2005). The impact of influenza on the health and health care utilisation of elderly people. Vaccine *23*, S1–S9. https://doi.org/10.1016/j.vaccine.2005.04.018.
8. Mohrin, M., Shin, J., Liu, Y., Brown, K., Luo, H., Xi, Y., Haynes, C.M., and Chen, D. (2015). Stem cell aging. A mitochondrial UPR-mediated metabolic checkpoint regulates hematopoietic stem cell aging. Science *347*, 1374–1377. https://doi.org/10.1126/science.aaa2361.
9. Luo, H., Mu, W.C., Karki, R., Chiang, H.H., Mohrin, M., Shin, J.J., Ohkubo, R., Ito, K., Kanneganti, T.D., and Chen, D. (2019). Mitochondrial Stress-Initiated Aberrant Activation of the NLRP3 Inflammasome Regulates the Functional Deterioration of Hematopoietic Stem Cell Aging. Cell Rep. *26*, 945–954.e4. https://doi.org/10.1016/j.celrep.2018.12.101.
10. Ho, T.T., Warr, M.R., Adelman, E.R., Lansinger, O.M., Flach, J., Verovskaya, E.V., Figueroa, M.E., and Passegué, E. (2017). Autophagy maintains the metabolism and function of young and old stem cells. Nature *543*, 205–210. https://doi.org/10.1038/nature21388.
11. Florian, M.C., Dörr, K., Niebel, A., Daria, D., Schrezenmeier, H., Rojewski, M., Filippi, M.D., Hasenberg, A., Gunzer, M., Scharffetter-Kochanek, K., et al. (2012). Cdc42 activity regulates hematopoietic stem cell aging and rejuvenation. Cell Stem Cell *10*, 520–530. https://doi.org/10.1016/j.stem.2012.04.007.
12. Rossi, D.J., Bryder, D., Seita, J., Nussenzweig, A., Hoeijmakers, J., and Weissman, I.L. (2007). Deficiencies in DNA damage repair limit the function of haematopoietic stem cells with age. Nature *447*, 725–729. https://doi.org/10.1038/nature05862.
13. Mohrin, M., Bourke, E., Alexander, D., Warr, M.R., Barry-Holson, K., Le Beau, M.M., Morrison, C.G., and Passegué, E. (2010). Hematopoietic stem cell quiescence promotes error-prone DNA repair and mutagenesis. Cell Stem Cell *7*, 174–185. https://doi.org/10.1016/j.stem.2010.06.014.
14. Beerman, I., Seita, J., Inlay, M.A., Weissman, I.L., and Rossi, D.J. (2014). Quiescent hematopoietic stem cells accumulate DNA damage during aging that is repaired upon entry into cell cycle. Cell Stem Cell *15*, 37–50. https://doi.org/10.1016/j.stem.2014.04.016.
15. Nijnik, A., Woodbine, L., Marchetti, C., Dawson, S., Lambe, T., Liu, C., Rodrigues, N.P., Crockford, T.L., Cabuy, E., Vindigni, A., et al. (2007). DNA repair is limiting for haematopoietic stem cells during ageing. Nature *447*, 686–690. https://doi.org/10.1038/nature05875.
16. Gutierrez-Martinez, P., Hogdal, L., Nagai, M., Kruta, M., Singh, R., Sarosiek, K., Nussenzweig, A., Beerman, I., Letai, A., and Rossi, D.J. (2018). Diminished apoptotic priming and ATM signalling confer a survival advantage onto aged haematopoietic stem cells in response to DNA damage. Nat. Cell Biol. *20*, 413–421. https://doi.org/10.1038/s41556-018-0054-y.
17. Kusumbe, A.P., Ramasamy, S.K., Itkin, T., Mäe, M.A., Langen, U.H., Betsholtz, C., Lapidot, T., and Adams, R.H. (2016). Age-dependent modulation of vascular niches for haematopoietic stem cells. Nature *532*, 380–384. https://doi.org/10.1038/nature17638.
18. Ho, Y.H., Del Toro, R., Rivera-Torres, J., Rak, J., Korn, C., García-García, A., Macías, D., González-Gómez, C., Del Monte, A., Wittner, M., et al. (2019). Remodeling of Bone Marrow Hematopoietic Stem Cell Niches Promotes Myeloid Cell Expansion during Premature or Physiological Aging. Cell Stem Cell *25*, 407–418.e6. https://doi.org/10.1016/j.stem.2019.06.007.
19. Ambrosi, T.H., Marecic, O., McArdle, A., Sinha, R., Gulati, G.S., Tong, X., Wang, Y., Steininger, H.M., Hoover, M.Y., Koepke, L.S., et al. (2021). Aged skeletal stem cells

generate an inflammatory degenerative niche. Nature *597*, 256–262. https://doi.org/10.1038/s41586-021-03795-7.

20. Maryanovich, M., Zahalka, A.H., Pierce, H., Pinho, S., Nakahara, F., Asada, N., Wei, Q., Wang, X., Ciero, P., Xu, J., et al. (2018). Adrenergic nerve degeneration in bone marrow drives aging of the hematopoietic stem cell niche. Nat. Med. *24*, 782–791. https://doi.org/10.1038/s41591-018-0030-x.
21. Ramalingam, P., Poulos, M.G., Gutkin, M.C., Katsnelson, L., Freire, A.G., Lazzari, E., and Butler, J.M. (2020). Endothelial mTOR maintains hematopoiesis during aging. J. Exp. Med. *217*, e20191212. https://doi.org/10.1084/jem.20191212.
22. Poulos, M.G., Ramalingam, P., Gutkin, M.C., Llanos, P., Gilleran, K., Rabbany, S.Y., and Butler, J.M. (2017). Endothelial transplantation rejuvenates aged hematopoietic stem cell function. J. Clin. Invest. *127*, 4163–4178. https://doi.org/10.1172/JCI93940.
23. Guidi, N., Sacma, M., Ständker, L., Soller, K., Marka, G., Eiwen, K., Weiss, J.M., Kirchhoff, F., Weil, T., Cancelas, J.A., et al. (2017). Osteopontin attenuates aging-associated phenotypes of hematopoietic stem cells. EMBO J. *36*, 1463. https://doi.org/10.15252/embj.201796968.
24. Mitchell, C.A., Verovskaya, E.V., Calero-Nieto, F.J., Olson, O.C., Swann, J.W., Wang, X., Hérault, A., Dellorusso, P.V., Zhang, S.Y., Svendsen, A.F., et al. (2023). Stromal niche inflammation mediated by IL-1 signalling is a targetable driver of haematopoietic ageing. Nat. Cell Biol. *25*, 30–41. https://doi.org/10.1038/s41556-022-01053-0.
25. Young, K., Eudy, E., Bell, R., Loberg, M.A., Stearns, T., Sharma, D., Velten, L., Haas, S., Filippi, M.D., and Trowbridge, J.J. (2021). Decline in IGF1 in the bone marrow microenvironment initiates hematopoietic stem cell aging. Cell Stem Cell *28*, 1473–1482.e7. https://doi.org/10.1016/j.stem.2021.03.017.
26. Ramalingam, P., Gutkin, M.C., Poulos, M.G., Tillery, T., Doughty, C., Winiarski, A., Freire, A.G., Rafii, S., Redmond, D., and Butler, J.M. (2023). Restoring bone marrow niche function rejuvenates aged hematopoietic stem cells by reactivating the DNA Damage Response. Nat. Commun. *14*, 2018. https://doi.org/10.1038/s41467-023-37783-4.
27. Kuribayashi, W., Oshima, M., Itokawa, N., Koide, S., Nakajima-Takagi, Y., Yamashita, M., Yamazaki, S., Rahmutulla, B., Miura, F., Ito, T., et al. (2021). Limited rejuvenation of aged hematopoietic stem cells in young bone marrow niche. J. Exp. Med. *218*, e20192283. https://doi.org/10.1084/jem.20192283.
28. Ho, T.T., Dellorusso, P.V., Verovskaya, E.V., Bakker, S.T., Flach, J., Smith, L.K., Ventura, P.B., Lansinger, O.M., Hérault, A., Zhang, S.Y., et al. (2021). Aged hematopoietic stem cells are refractory to bloodborne systemic rejuvenation interventions. J. Exp. Med. *218*, e20210223. https://doi.org/10.1084/jem.20210223.
29. Sun, D., Luo, M., Jeong, M., Rodriguez, B., Xia, Z., Hannah, R., Wang, H., Le, T., Faull, K.F., Chen, R., et al. (2014). Epigenomic profiling of young and aged HSCs reveals concerted changes during aging that reinforce self-renewal. Cell Stem Cell *14*, 673–688. https://doi.org/10.1016/j.stem.2014.03.002.
30. Beerman, I., Bock, C., Garrison, B.S., Smith, Z.D., Gu, H., Meissner, A., and Rossi, D.J. (2013). Proliferation-dependent alterations of the DNA methylation landscape underlie hematopoietic stem cell aging. Cell Stem Cell *12*, 413–425. https://doi.org/10.1016/j.stem.2013.01.017.
31. Wahlestedt, M., Norddahl, G.L., Sten, G., Ugale, A., Frisk, M.A.M., Mattsson, R., Deierborg, T., Sigvardsson, M., and Bryder, D. (2013). An epigenetic component of hematopoietic stem cell aging amenable to reprogramming into a young state. Blood *121*, 4257–4264. https://doi.org/10.1182/blood-2012-11-469080.
32. Termini, C.M., Pang, A., Fang, T., Roos, M., Chang, V.Y., Zhang, Y., Setiawan, N.J., Signaevskaia, L., Li, M., Kim, M.M., et al. (2021). Neuropilin 1 regulates bone marrow vascular regeneration and hematopoietic reconstitution. Nat. Commun. *12*, 6990. https://doi.org/10.1038/s41467-021-27263-y.
33. Himburg, H.A., Sasine, J., Yan, X., Kan, J., Dressman, H., and Chute, J.P. (2016). A Molecular Profile of the Endothelial Cell Response to Ionizing Radiation. Radiat. Res. *186*, 141–152. https://doi.org/10.1667/RR14444.1.
34. Fang, T., Zhang, Y., Chang, V.Y., Roos, M., Termini, C.M., Signaevskaia, L., Quarmyne, M., Lin, P.K., Pang, A., Kan, J., et al. (2020). Epidermal growth factor receptor-dependent DNA repair promotes murine and human hematopoietic regeneration. Blood *136*, 441–454. https://doi.org/10.1182/blood.2020005895.
35. Chambers, S.M., Shaw, C.A., Gatza, C., Fisk, C.J., Donehower, L.A., and Goodell, M.A. (2007). Aging hematopoietic stem cells decline in function and exhibit epigenetic dysregulation. PLoS Biol. *5*, e201. https://doi.org/10.1371/journal.pbio.0050201.
36. Rossi, D.J., Bryder, D., Zahn, J.M., Ahlenius, H., Sonu, R., Wagers, A.J., and Weissman, I.L. (2005). Cell intrinsic alterations underlie hematopoietic stem cell aging. Proc. Natl. Acad. Sci. USA *102*, 9194–9199. https://doi.org/10.1073/pnas.0503280102.
37. Osawa, M., Hanada, K., Hamada, H., and Nakauchi, H. (1996). Long-term lymphohematopoietic reconstitution by a single CD34-low/negative hematopoietic stem cell. Science *273*, 242–245. https://doi.org/10.1126/science.273.5272.242.
38. Klaude, M., Eriksson, S., Nygren, J., and Ahnström, G. (1996). The comet assay: mechanisms and technical considerations. Mutat. Res. *363*, 89–96. https://doi.org/10.1016/0921-8777(95)00063-1.
39. Weinstock, D.M., Brunet, E., and Jasin, M. (2007). Formation of NHEJ-derived reciprocal chromosomal translocations does not require Ku70. Nat. Cell Biol. *9*, 978–981. https://doi.org/10.1038/ncb1624.
40. Ferguson, D.O., Sekiguchi, J.M., Chang, S., Frank, K.M., Gao, Y., DePinho, R.A., and Alt, F.W. (2000). The nonhomologous end-joining pathway of DNA repair is required for genomic stability and the suppression of translocations. Proc. Natl. Acad. Sci. USA *97*, 6630–6633. https://doi.org/10.1073/pnas.110152897.
41. Chang, H.H.Y., Watanabe, G., Gerodimos, C.A., Ochi, T., Blundell, T.L., Jackson, S.P., and Lieber, M.R. (2016). Different DNA End Configurations Dictate Which NHEJ Components Are Most Important for Joining Efficiency. J. Biol. Chem. *291*, 24377–24389. https://doi.org/10.1074/jbc.M116.752329.
42. Zhang, X., Li, J., Sejas, D.P., and Pang, Q. (2005). Hypoxia-reoxygenation induces premature senescence in FA bone marrow hematopoietic cells. Blood *106*, 75–85.
43. Sera, Y., Nakata, Y., Ueda, T., Yamasaki, N., Koide, S., Kobayashi, H., Ikeda, K.I., Kobatake, K., Iwasaki, M., Oda, H., et al. (2021). UTX maintains the functional integrity of the murine hematopoietic system by globally regulating aging-associated genes. Blood *137*, 908–922.
44. Pang, W.W., Price, E.A., Sahoo, D., Beerman, I., Maloney, W.J., Rossi, D.J., Schrier, S.L., and Weissman, I.L. (2011). Human bone marrow hematopoietic stem cells are increased in frequency and myeloid-biased with age. Proc. Natl. Acad. Sci. USA *108*, 20012–20017. https://doi.org/10.1073/pnas.1116110108.
45. Fast, E.M., Sporrij, A., Manning, M., Rocha, E.L., Yang, S., Zhou, Y., Guo, J., Baryawno, N., Barkas, N., Scadden, D., et al. (2021). External signals regulate continuous transcriptional states in hematopoietic stem cells. Elife *10*, e66512. https://doi.org/10.7554/eLife.66512.
46. Renders, S., Svendsen, A.F., Panten, J., Rama, N., Maryanovich, M., Sommerkamp, P., Ladel, L., Redavid, A.R., Gibert, B., Lazare, S., et al. (2021). Niche derived netrin-1 regulates hematopoietic stem cell dormancy via its receptor neogenin-1. Nat. Commun. *12*, 608. https://doi.org/10.1038/s41467-020-20801-0.
47. Min, I.M., Pietramaggiori, G., Kim, F.S., Passegué, E., Stevenson, K.E., and Wagers, A.J. (2008). The transcription factor EGR1 controls both the proliferation and localization of hematopoietic stem cells. Cell Stem Cell *2*, 380–391. https://doi.org/10.1016/j.stem.2008.01.015.
48. Yilmaz, O.H., Valdez, R., Theisen, B.K., Guo, W., Ferguson, D.O., Wu, H., and Morrison, S.J. (2006). Pten dependence distinguishes haematopoietic stem cells from leukaemia-initiating cells. Nature *441*, 475–482.
49. Nguyen, N.Y.N., Maxwell, M.J., Ooms, L.M., Davies, E.M., Hilton, A.A., Collinge, J.E., Hilton, D.J., Kile, B.T., Mitchell, C.A., Hibbs, M.L., et al. (2011). An ENU-induced mouse mutant of SHIP1 reveals a critical role of the stem cell isoform for suppression of macrophage activation. Blood *117*, 5362–5371. https://doi.org/10.1182/blood-2011-01-331041.
50. Lopez, R.A., Schoetz, S., DeAngelis, K., O'Neill, D., and Bank, A. (2002). Multiple hematopoietic defects and delayed globin switching in Ikaros null mice. Proc. Natl. Acad. Sci. USA *99*, 602–607. https://doi.org/10.1073/pnas.022412699.
51. Yue, W., Pi, Q.M., Zhang, W.J., Zhou, G.D., Cui, L., Liu, W., and Cao, Y. (2010). Platelet endothelial cell adhesion molecule-1, stage-specific embryonic antigen-1, and Flk-1 mark distinct populations of mouse embryonic stem cells during differentiation toward hematopoietic/endothelial cells. Stem Cells Dev. *19*, 1937–1948. https://doi.org/10.1089/scd.2010.0096.
52. Maglitto, A., Mariani, S.A., de Pater, E., Rodriguez-Seoane, C., Vink, C.S., Piao, X., Lukke, M.L., and Dzierzak, E. (2021). Unexpected redundancy of Gpr56 and Gpr97 during hematopoietic cell development and differentiation. Blood Adv. *5*, 829–842. https://doi.org/10.1182/bloodadvances.2020003693.
53. Zhang, M.J., Pisco, A.O., Darmanis, S., and Zou, J. (2021). Mouse aging cell atlas analysis reveals global and cell-type specific aging signatures. Elife *10*, e62293.

54. Vasile, E., Tomita, Y., Brown, L.F., Kocher, O., and Dvorak, H.F. (2001). Differential expression of Thymosin β-10 by early passage and senescent vascular endothelium is modulated by VPF/VEGF: evidence for senescent endothelial cells *in vivo* at sites of atherosclerosis. Faseb. J. *15*, 458–466.
55. Lee, S.S., Lee, R.Y.N., Fraser, A.G., Kamath, R.S., Ahringer, J., and Ruvkun, G. (2003). A systematic RNAi screen identifies a critical role for mitochondria in C. elegans longevity. Nat. Genet. *33*, 40–48.
56. Florian, M.C., Dörr, K., Niebel, A., Daria, D., Schrezenmeier, H., Rojewski, M., Filippi, M.D., Hasenberg, A., Gunzer, M., Scharffetter-Kochanek, K., et al. (2012). Cdc42 activity regulates hematopoietic stem cell aging and rejuvenation. Cell Stem Cell *10*, 520–530.
57. Feng, L., Huang, J., and Chen, J. (2009). MERIT40 facilitates BRCA1 localization and DNA damage repair. Genes Dev. *23*, 719–728.
58. Kim, K.H., and Roberts, C.W.M. (2014). Mechanisms by which Smarcb1 loss drives rhabdoid tumor growth. Cancer Genet. *207*, 365–372.
59. Baron, V., Adamson, E.D., Calogero, A., Ragona, G., and Mercola, D. (2006). The transcription factor Egr1 is a direct regulator of multiple tumor suppressors including TGFbeta1, PTEN, p53, and fibronectin. Cancer Gene Ther. *13*, 115–124.
60. Rosivatz, E., Matthews, J.G., McDonald, N.Q., Mulet, X., Ho, K.K., Lossi, N., Schmid, A.C., Mirabelli, M., Pomeranz, K.M., Erneux, C., et al. (2006). A small molecule inhibitor for phosphatase and tensin homologue deleted on chromosome 10 (PTEN). ACS Chem. Biol. *1*, 780–790.
61. Wilson, A., Laurenti, E., Oser, G., van der Wath, R.C., Blanco-Bose, W., Jaworski, M., Offner, S., Dunant, C.F., Eshkind, L., Bockamp, E., et al. (2008). Hematopoietic stem cells reversibly switch from dormancy to self-renewal during homeostasis and repair. Cell *135*, 1118–1129. https://doi.org/10.1016/j.cell.2008.10.048.
62. Koschmieder, S., Göttgens, B., Zhang, P., Iwasaki-Arai, J., Akashi, K., Kutok, J.L., Dayaram, T., Geary, K., Green, A.R., Tenen, D.G., and Huettner, C.S. (2005). Inducible chronic phase of myeloid leukemia with expansion of hematopoietic stem cells in a transgenic model of BCR-ABL leukemogenesis. Blood *105*, 324–334. https://doi.org/10.1182/blood-2003-12-4369.
63. Roh, M., Paterson, A.J., Asa, S.L., Chin, E., and Kudlow, J.E. (2001). Stage-sensitive blockade of pituitary somatomammotrope development by targeted expression of a dominant negative epidermal growth factor receptor in transgenic mice. Mol. Endocrinol. *15*, 600–613. https://doi.org/10.1210/mend.15.4.0625.
64. Beerman, I., Bhattacharya, D., Zandi, S., Sigvardsson, M., Weissman, I.L., Bryder, D., and Rossi, D.J. (2010). Functionally distinct hematopoietic stem cells modulate hematopoietic lineage potential during aging by a mechanism of clonal expansion. Proc. Natl. Acad. Sci. USA *107*, 5465–5470. https://doi.org/10.1073/pnas.1000834107.
65. Janzen, V., Forkert, R., Fleming, H.E., Saito, Y., Waring, M.T., Dombkowski, D.M., Cheng, T., DePinho, R.A., Sharpless, N.E., and Scadden, D.T. (2006). Stem-cell ageing modified by the cyclin-dependent kinase inhibitor p16INK4a. Nature *443*, 421–426. https://doi.org/10.1038/nature05159.
66. Rossi, D.J., Bryder, D., and Weissman, I.L. (2007). Hematopoietic stem cell aging: mechanism and consequence. Exp. Gerontol. *42*, 385–390. https://doi.org/10.1016/j.exger.2006.11.019.
67. Waldrip, Z.J., Burdine, L., Harrison, D.K., Azevedo-Pouly, A.C., Storey, A.J., Moffett, O.G., Mackintosh, S.G., and Burdine, M.S. (2021). DNA-PKcs kinase activity stabilizes the transcription factor Egr1 in activated immune cells. J. Biol. Chem. *297*, 101209. https://doi.org/10.1016/j.jbc.2021.101209.
68. Ross, J.B., Myers, L.M., Noh, J.J., Collins, M.M., Carmody, A.B., Messer, R.J., Dhuey, E., Hasenkrug, K.J., and Weissman, I.L. (2024). Depleting myeloid-biased haematopoietic stem cells rejuvenates aged immunity. Nature *628*, 162–170.
69. Lytal, N., Ran, D., and An, L. (2020). Normalization Methods on Single-Cell RNA-seq Data: An Empirical Survey. Front. Genet. *11*, 41. https://doi.org/10.3389/fgene.2020.00041.

STAR★METHODS

KEY RESOURCES TABLE

REAGENT or RESOURCE	SOURCE	IDENTIFIER
Antibodies		
V450 mouse lineage antibody cocktail	BD Biosciences	561301
Rat anti-mouse c-kit/CD117-PE	BD Biosciences	553355
Rat anti-mouse Sca-1 (Ly-6A/E)-APC-Cy7	BioLegend	108126
Rat anti-mouse CD34-AF647	BD Biosciences	560230
Rat anti-mouse CD48-FITC	BD Biosciences	557484
Rat anti-mouse CD150-BV605	BioLegend	115927
PE Mac-1 (CD11b)	BD Biosciences	557397
PE Gr-1 (Ly-6G and Ly-6C)	BD Biosciences	553128
APC Ter-119	BD Biosciences	557909
APC-Cy7 B220 (CD45R)	BD Biosciences	552094
V450 CD3	BD Biosciences	561389
Brilliant Violet 605 anti-mouse CD45.1	BioLegend	110738
FITC anti-mouse-CD45.2	BD Biosciences	553772
Rat anti-mouse CD48-AF700	BioLegend	103426
Rat anti-mouse CD150-PerCP-Cy5.5	BioLegend	115921
BD Pharmingen™ Purified Rat Anti-Mouse CD16/CD32	BD Biosciences	553142
FITC anti-EGFR antibody	Abcam	ab11400
Rabbit anti-EGFR (phospho Y1173) antibody	Abcam	ab5652
FITC p-EGFR (Tyr1068) Recombinant Rabbit mAb	ThermoFisher	MA5-27995
AF488 anti-H2A.X (phosphor-Ser139) (1:25)	BioLegend	613406
AF-488 goat anti-rabbit secondary antibody	ThermoFisher	A27034
rabbit anti-DNA-PKcs (p-Thr2609) primary antibody (1:100)	Novus Biological	NDP1-02456
rabbit p-Artemis (Ser516) antibody (1:100)	ThermoFisher	PA5-36778
Ly-6A/E (Sca-1) Monoclonal Antibody (D7), Alexa Fluor 700	eBioscience	5016926
CD117 (c-Kit) Monoclonal Antibody (2B8), APC-eFluor 780	eBioscience	501129685
PE/Cyanine7 anti-mouse CD150 (SLAM) Antibody	Biolegend	115914
BD OptiBuild™ BV605 Hamster Anti-Mouse CD48	BD Biosciences	740353
CD229 Recombinant Rabbit Monoclonal Antibody, APC	ThermoFisher	MA5-46833
Chemicals, peptides, and recombinant proteins		
7AAD	BD Biosciences	559925
Recombinant mouse EGF	R&D Systems	2028-EG
Recombinant Mouse Thrombopoietin Protein, CF	R&D Systems	488-TO/CF
Recombinant Mouse SCF Protein, CF	R&D Systems	455-MC/CF
Recombinant Mouse Flt-3, CF	R&D Systems	427-FL/CF
IMDM	Gibco	12440053
X-VIVO 15 Serum-free Hematopoietic Cell Media	Lonza	04-418Q
Hyclone Fetal Bovine Serum	Cytiva	SH30071.03
Penicillin-Streptomycin	Gibco	15140148
MethoCult™ GF M3434	Stemcell Technologies	03434
Bovine serum albumin solution, 10% in PBS	Millipore	SLCQ2577
MK-2206 2HCl	Selleckchem	S1078

(*Continued on next page*)

Continued

REAGENT or RESOURCE	SOURCE	IDENTIFIER
NU7441 (KU-57788)	Selleckchem	S2638
VO-Ohpic trihydrate	MedChemExpress	HY-13074
Doxycycline	Sigma-Aldrich	24390-14-5
Critical commercial assays		
Mouse EGF DuoSet ELISA kit	R&D Systems	DY2028
Mouse Betacellulin DuoSet ELISA kit	R&D Systems	DY1025
Mouse HB-EGF DuoSet ELISA kit	R&D Systems	DY8239-05
DuoSet ancillary Reagent Kit 2	R&D Systems	DY008
RNeasy Micro Kit	Qiagen	74004
High-Capacity cDNA Reverse Transcription Kit	ThermoFisher	4368814
TaqMan Universal PCR Master Mix	ThermoFisher	4304437
Lineage Depletion Kit, Mouse	Miltenyi Biotec	130-090-858
BD Pharmingen FITC mouse anti-Ki67 set	BD Biosciences	556026
BD Pharmingen PE Annexin V apoptosis detection Kit I	BD Biosciences	559763
CometAssay Kit	R&D Systems	4250-050K
LS Columns	Miltenyi Biotec	130-042-401
BD Cytofix/Cytoperm kit	BD Biosciences	554714
Deposited data		
RNA sequence data	GEO Database	GSE266959
RNA sequence data	GEO Database	GSE252293
Experimental models: Organisms/strains		
Mouse: C57Bl/6J	The Jackson Laboratory	000664
Mouse: B6.SJL-Ptprca Pepcb/BoyJ	The Jackson Laboratory	002014
Tal1-tTA (SCL-tTA, B6.Cg-Tg (Tal1-tTA)19Dgt/J) mice	The Jackson Laboratory	017722
TRE-EGFRtr (B6;SJL-Tg(tetO-Egfr*)2-9Jek/J) mice	The Jackson Laboratory	010575
Oligonucleotides		
Mouse Gapdh FAM	ThermoFisher	Mm99999915_g1
Mouse egfr FAM	ThermoFisher	Mm01187861_m1
Mouse Egr1 FAM	ThermoFisher	Mm00656724_m1
Mouse EGFR intracellular domain FAM	ThermoFisher	Mm01187868_m1
Mouse EGFR extracellular domain FAM	ThermoFisher	Mm01187861_m1
Software and algorithms		
Ingenuity Pathway Analysis (IPA)	QIAGEN	
GraphPad Prism 9	GraphPad	https://www.graphpad.com/
FlowJo	FlowJo	https://www.flowjo.com/
CometAssay Analysis Software	R&D systems	4260-000-CS

RESOURCE AVAILABILITY

Lead contact

Further information and requests for resources and reagents should be directed to and will be fulfilled by the lead contact, John P. Chute (john.chute@cshs.org).

Materials availability

All materials generated in this study will be available from the lead contact upon request.

Data and code availability

- RNA-seq data is deposited at GEO: GSE266959 and GSE252293 and are publicly available as of the date of publication.
- There is no original code in this publication.
- Any additional information required to reanalyze the data reported in this paper is available from the lead contact upon request.

EXPERIMENTAL MODEL AND STUDY PARTICIPANT DETAILS

Mice

All animal procedures were performed under protocols approved by the Cedars Sinai Medical Center Animal Care and Use Committee (J.P.C., #009617) and the UCLA animal care and use committee (J.P.C., #2014-021-21). Young *C57Bl6* (6-8 weeks) and *B6.SJL* mice, 8-16 weeks of age, were obtained from Jackson Laboratory (Bar Harbor, ME) and the UCLA Radiation Oncology Animal core. Aged, female *C57Bl6* mice were 18-22 months of age and were obtained from the National Institute of Aging. Middle aged mice were 12-15 months of age. *Tal1-tTA* and *TRE-EGFR-tr* mice were purchased from Jackson Laboratories. Mice were genotyped for the *Tal1-tTA* transgene and *TRE-EGFR-tr* transgene by Transnetyx (Cordova, TN). Male and female littermates with genotype *Tal1-tTA+/TRE-EGFR-tr+* genotype were maintained on or off 0.2g/L doxycycline (Sigma Aldrich, St. Louis, MO) in drinking water from birth, changed weekly. For *in vivo* gain-of-function studies, 1 μg/g of recombinant EGF in 200μl saline was injected intra-peritoneally (IP) every other day for 6 weeks in aged mice. At the end of 6 weeks, mice were sacrificed and analyzed with complete blood counts, BM flow cytometric analyses for HSC content and lineage markers, Colony forming cell (CFC) assays and competitive repopulation assays, and markers of senescence.

Cell culture

Sorted BM KSL and 34^-KSL cells were cultured in IMDM media with 10% FBS and 1% penicillin-streptomycin plus thrombopoietin (20 ng/ml), stem cell factor (SCF, 125 ng/ml) and Flt3 ligand (50 ng/ml) (TSF media) as indicated in U-shape 96-well plates in a humidified tissue culture incubator with 5% CO_2. Where it is indicated, cells were treated with EGF or PBS as control and in some cases with or without inhibitors.

METHOD DETAILS

Competitive repopulation assay

Competitive repopulation assays were performed by tail vein injection of 3 x 10^4 donor BM cells from $CD45.2^+$ *C57Bl6* mice into lethally irradiated (900 cGy) congenic $CD45.1^+$ *B6.SJL* mice, along with host 2x10^5 $CD45.1^+$ BM competitor cells. Donor engraftment and lineage differentiation were assessed every 4 weeks by peripheral blood (PB) flow cytometric analysis. At 16 weeks, analysis of donor cell chimerism in BM hematopoietic stem/progenitor cells (HSPCs) was also performed. Secondary transplants were performed with 3 million BM donor cells transplanted into lethally irradiated recipient mice, along with 2x10^5 $CD45.1^+$ BM competitor cells. Secondary engraftment and lineage chimerism were assessed every 4 weeks following second transplantation though week 16, at which point BM analyses were conducted as described for the end of primary time point.

Single cell RNA sequencing

For single-cell RNA sequencing (scRNA-seq), BM $CD34^-$KSL cells were sorted from mice after subcutaneous injection of 1 μg/g EGF or saline in 200 μL daily for 3 days. RNA was extracted using the Chromium Single Cell 3' V2 Reagents Kits. The libraries were sequenced on the NovaSeq 6000 platform. Sequence reads were aligned and analyzed using the Cell Ranger Count pipeline (v7.0.1) (10X Genomics) to generate cell-associated gene expression matrices. The expression data was then normalized via Scran deconvolution[69] and differential expression among samples was measured with DESeq 2 algorithm in Partek Flow. UMAP plots were generated in R v4.2.2 using the Seurat v4.2.1 package following dimensionality reduction using the first ten principal components while density plots were generated using ggplot2 v3.4.0 and the stat_density_2d function. Statistical filters of $p < 0.05$, FDR < 0.05, and fold change > 1.5X were applied prior to Ingenuity Pathway Analysis.

ELISA of EGF receptor ligands

Mouse EGF, HB-EGF and Betacellulin were measured in the serum and BM supernatant of young and aged mice using R&D Systems DuoSet ELISA Kits (Biotechne, Minneapolis, MN) according to the manufacturer's instructions. Concentrations of each ligand were calculated according to the standard curve generated for each set of samples according to the instructions.

Flow cytometric analyses and cell sorting

Flow cytometric cell sorting of bone marrow cells was performed using BD Influx cell sorter (Becton Dickinson, Franklin Lakes, NJ). Mouse PB was collected using EDTA as anticoagulant. Mouse BM cells were collected from femurs and tibia with IMDM supplemented with 10% FBS and 1% penicillin-streptomycin. Red blood cells (RBCs) were lysed with ACK lysing buffer (Quality Biological Inc, Gaithersburg, MD). Live cells were counted using trypan blue exclusion and BioRad TC20 automated cell counter.

Lineage analysis was performed using PE Mac-1 (CD11b) (Cat # 557397), PE Gr-1 (Ly-6G and Ly-6C) (553128), APC Ter-119 (557909), V450 CD3 (561389), APC-Cy7 B220 (CD45R) (552094) antibodies purchased from BD Biosciences, San Jose, CA. For donor cell engraftment analyses in transplanted mice, Brilliant Violet 605 (BV605)-CD45.1 (BioLegend) and FITC-CD45.2 (BD Biosciences) antibodies were used to distinguish

donor cells from recipient and competitor cells. Lineage depletion of BM cells was performed using Direct Lineage Cell Depletion Kit and LS columns (Miltenyi Biotec, Germany) according to the manufacturer's instructions. Lineage-depleted BM cells were stained with V450 mouse lineage antibody cocktail (BD Biosciences), rat anti-mouse c-kit/CD117-PE (BD Biosciences), Sca-1 (Ly-6A/E)-APC-Cy7 (BioLegend) and CD34-AF647 (BD Biosciences) antibodies for analysis of ckit$^+$sca-1$^+$lineage$^-$CD34$^-$ (CD34$^-$KSL) and CD34$^+$KSL cells. Lineage-depleted BM cells were stained with V450 mouse lineage antibody cocktail (BD Biosciences), APC-eFluor 780 c-Kit (eBioscience), Alexa Fluor 700 Sca-1 (eBioscience), PE-Cyanine7 CD150 (Biolegend), BV605 CD48 (BD Biosciences) APC CD229 (Invitrogen) antibodies for analysis of ckit$^+$sca-1$^+$lineage$^-$CD48$^-$CD150$^+$CD229$^-$ (Myeloid-biased SLAM KSL). For donor cell engraftment analyses in transplanted mice, BV605-CD45.1 (Biolegend) and FITC-CD45.2 (BD Biosciences) antibodies were used to distinguish donor cells from recipient/competitor cells; and rat anti-mouse CD48-AF700 and CD150-PerCP-Cy5.5 (BioLegend) antibodies were used for analysis of BM HSCs.

For EGF receptor (EGFR) expression and phosphorylation (p-EGFR) and γ-H2AX analyses in CD34$^-$KSL HSCs, BM cells were isolated in X-VIVO 15 Serum-free Hematopoietic Cell Media (Lonza, Walkersville, MD). After lineage depletion, cells were stained at 4°C for 30 min to label CD34$^-$KSL cells. To analyze ERGR expression, the stained cells were washed with PBS and immediately fixed and permeabilized using BD Cytofix/Cytoperm kit (BD Biosciences). To perform p-EGFR and γ-H2AX analysis, the stained cells were washed and starved in no-serum IMDM media at 37°C for 1 hour followed by treatment with EGF at 20 ng/ml or 100 ng/ml at 37°C for 15 min or 2 hours as indicated in figure legend, then the cells were immediately fixed and permeabilized using the BD Cytofix/Cytoperm kit. The fixed and permeabilized cells in Perm/Wash buffer (BD Biosciences) were blocked with mouse Fc Block (BD Pharmingen™ Purified Rat Anti-Mouse CD16/CD32) at room temperature (RT) for 15 min. EGFR protein was labeled using FITC anti-EGFR antibody (1:100, ab11400, Abcam, Cambridge, United Kingdom) at 4°C for 30 min; for analysis of EGFR phosphorylation at Y1068, we used FITC rabbit p-EGFR (Y1068) monoclonal antibody (MA5-27995, Thermo Fisher) overnight at 4°C, and EGFR p-Y1173 analysis was performed using rabbit anti-mouse p-EGFR (Y1173) primary antibody (1:100, ab562, Abcam) overnight at 4°C, followed by AF-488 goat anti-rabbit secondary antibody (1:2000, A27034, ThermoFisher) at RT for 30 min. For γ-H2AX analysis, the cells were stained with AF488 anti-H2AX (phosphor-Ser139) (5ul/test, cat # 613406, BioLegend).

To analyze phosphorylation of DNA-PKcs (p-DNA-PKcs) and Artemis (p-Artemis), RBC-lysed BM cells were stained for KSL HSPCs and followed by starvation in no-serum IMDM at 37°C for 1 hr, then cells were treated with EGF at 10 ng/ml for 5 min and were immediately fixed and permeabilized and then blocked as stated above. Analysis of p-DNA-PKcs was performed with rabbit anti-DNA-PKcs (p-Thr2609) primary antibody (1:100, ab562, Abcam) and p-Artemis was stained with rabbit p-Artemis (Ser516) antibody (1:100, #NDP1-02456, Novus Biological, Centennial, CO) for 1 hour at 4°C followed by AF-488 goat anti-rabbit secondary antibody (1:1000, A27034, ThermoFisher) at 4°C for 1 h. All stained cells were washed and analyzed for percentage or mean fluorescence intensity (MFI) of parental cell population. All flow cytometric analyses were performed on a BD Canto II or Symphony FACS instrument with BD FACS DIVA software (BD Biosciences, San Jose, CA) and FlowJo software (FlowJo, Ashland, OR).

qRTPCR

Total RNA was prepared using the RNeasy Micro Kit per the manufacturer's instructions (QIAGEN, Hilden, Germany). RNA was reverse transcribed into cDNA using the High-Capacity cDNA Reverse Transcription Kit (ThermoFisher Scientific, Canoga Park, CA). Real time PCR reaction was performed using Taqman Universal Master Mix and Taqman Gene Expression Assay primers (ThermoFisher) and analyzed using an Applied Biosystems QuantStudio 6 PCR Machine (ThermoFisher). All samples were determined with at least 3 replicates and GAPDH was used for gene expression normalization. Relative gene expression was analyzed using the $2^{-\Delta\Delta CT}$ method.

Comet assay

BM CD34$^-$KSL cells were analyzed immediately after sorting or after cultured with EGF in the presence or absence of 0.5 μM MK-2206, an allosteric AKT inhibitor (Selleckchem, Houston, TX) in TSF media for 1 hour at 37°C. Alkaline comet assay was performed using the Comet assay kit (R&D Systems). Slides were stained with Vista Green DNA Dye (Cell biolabs Inc, Chicago, IL) and comet tails were visualized and photographed at 40x magnification using EVOS M5000 Imaging System (ThermoFisher Scientific). Images were analyzed with the Comet analysis software (R&D systems).

Cell cycle and apoptosis assays

Sorted BM CD34$^-$KSL cells (4000 cells/well) were cultured in TSF media with or without EGF at 100 ng/ml in U-shape 96-well plates for 72 hr at 37°C. Cells were counted and stained for KSL cell surface markers followed by cell cycle analysis with FITC mouse anti-Ki67/7AAD staining kit (BD Biosciences) or cell apoptosis analysis using Annexin V/Propidium Iodide apoptosis detection kit (BD BioSciences).

CFC assay

CFC assays were performed as previously described.[34] Cells were counted and plated in MethoCult (StemCell Technologies, Vancouver, BC, Canada). EGF 100ng/ml and 10μM KU-60019 were added directly to MethoCult at the time of plating. Cells were cultured at 37°C, 5% CO_2 and counted on day 14 for colony forming unit- granulocyte monocyte (CFU-GMs), burst forming unit- erythroid (BFU-Es), and colony forming unit- granulocyte, erythroid, monocyte, megakaryocyte (CFU-GEMMs).

Transplantation assays

Limiting dose survival analysis was performed in recipient mice irradiated with split-dose (600 cGy and 575 cGy) TBI and transplanted with a limiting dose of 1 x 10^4 BM cells from *EGFR-WT* and *EGFR-DN* mice. Since *EGFR-DN* and *EGFR-WT* mice are mixed *C57BL/6* x *SJL* background, we utilized F1 progeny of *C57BL/6* mice x *SJL* mice as recipients. Mice were monitored daily for 30 days and euthanized according to our animal use protocol.

Immunofluorescence microscopy for γ-H2AX

Cells were plated on fibronectin-coated Nunc™ Lab-Tek™ II CC2™ Chamber Slide System (Thermo Fisher Scientific). After serum-starving for 45 min, cells were treated with 100 ng/mL EGF for 1hour. Cells were fixed with Fixation buffer (BD biosciences) for 10 minutes at room temperature, permeabilized with 0.5% Triton X-100 in PBS for 30 minutes, blocked for 30 minutes with 5% fetal bovine serum in perm buffer, and stained with Alexa Fluor 488 anti-H2A.X Phospho (Ser139) antibody (Biolegend) for 1hour at room temperature. Cells were mounted with Gold Antifade Reagent with DAPI (Cell Signaling Technology). Images were captured using the Leica Stellaris system (40x objective) and analyzed using ImageJ.

Bulk RNAseq

For bulk mRNA sequencing, BM CD34$^-$KSL cells were sorted from mice with Tal1-tTA+/TRE-EGFR-tr+ genotype that were maintained in drinking water with 0.2 g/L doxycycline (expressing wild-type EGFR only, EGFR-WT) or without doxycycline (except EGFR-WT, also expressing a cytoplasmic tyrosine kinase domain-deleted form of EGFR, EGFR-DN). Total RNA was prepared using Qiagen RNeasy Micro Kit (Qiagen). For mRNA-Seq Library prep, the SMART-Seq V4 Ultra Low RNA Input Kit for Sequencing (Takara Bio USA, Inc., Mountain View, CA) was used for reverse transcription and generation of double stranded cDNA for subsequent library preparation using the Nextera XT Library Preparation kit (Illumina, San Diego, CA). An input of 10 ng RNA was used for oligo(dT)-primed reverse transcription, followed by cDNA amplification and cleanup. Quantification of cDNA was performed using Qubit (Thermo Fisher Scientific). cDNA normalized to 80 pg/μl was fragmented and sequencing primers added simultaneously. A limiting-cycle PCR added Index 1 (i7) adapters, Index 2 (i5) adapters, and sequences required for cluster formation on the sequencing flow cell. Indexed libraries were pooled and cleaned up, and the pooled library size was verified on the 2100 Bioanalyzer (Agilent Technologies, Santa Clara, CA) and quantified via Qubit. Libraries were sequenced on a NovaSeq 6000 (Illumina) using with a 1x75 bp read length and coverage of over 30M reads/sample.

For data analysis, raw reads obtained from RNA-Seq were aligned and quantified using Illumina DRAGEN Bio-IT Platform RNA Pipeline (Illumina, USA) with the NCBI mouse mm39 transcriptome. Expression counts for each gene in all samples were normalized by a modified trimmed mean of the M-values normalization method and the unsupervised PC analysis (PCA) was performed with DESeq2 Bioconductor package version 1.40.2 in R version 4.3.1. Each gene was fitted into a negative binomial generalized linear model, and the Wald test was applied to assess the differential expressions between two sample groups by DESeq2. Benjamini and Hochberg procedure was applied to adjust for multiple hypothesis testing, and differential expression gene candidates were selected with a false discovery rate less than 0.05.

SA-β-Galactosidase assay

Cell senescence assay was performed using Cellular Senescence Live Cell Analysis Assay Kit (Cat # ENZ-KIT130-0010, Enzo Life Sciences, Farmingdale, NY) according to the instructions with some modifications, which measures senescence-associated β-galactosidase (SA-β-gal) activity in senescent cells using a fluorogenic substrate. Briefly, lineage-depleted mouse BM cells (0.2 x 10^6) were cultured in TSF media in the absence and presence of EGF (100 ng/ml) at 37°C for 24 h and cells were stained for CD34/KSL makers as described above. Cells were resuspended in 200 μl of 1X Cell Pretreatment Solution and pre-incubated at 37°C for 30 min, then cells were further incubated with SA-β-gal substrate at 37°C for 10 min by adding 0.5 μL of the provided 200X SA-β-Gal substrate solution directly to the cell suspension. Cells were washed 3 times with PBS and analyzed with flow cytometry.

Mitochondrial superoxide (MitoSOX) assay

MitoSOX measurement was performed using MitoSOX™ Red mitochondrial superoxide indicator for live-cell imaging kit (M36008, ThermoFisher Scientific) according to the instructions with minimum modifications. Briefly, lineage-depleted mouse BM cells (0.5 x 10^6) were cultured in TSF media in the absence and presence of EGF (100 ng/ml) at 37°C for 24 h and cells were stained for CD34/KSL makers as described above. Cells were resuspended in the concentration of 5 μM MitoSOX™ reagent working solution in Hank's balanced salt solution (HBSS) with calcium and magnesium and incubate for 10 minutes at 37°C, protected from light. Stained cells were washed, resuspended in the HBSS buffer and analyzed using flow cytometry.

QUANTIFICATION AND STATISTICAL ANALYSIS

All of the statistical details of experiments can be found in the Figure legends, including statistical tests used, n values, what n represents and precision measures. Data are shown as means or means ± SEM. Two-tailed t tests were used for simple comparisons. For multiple comparisons, one-way or two-way ANOVA was used to compare mean differences between groups. Where statistical tests are presented as asterisks or other symbols in Figures, each asterisk or symbol is defined in the relevant Figure Legend, along with the name of the statistical test. Survival analyses were performed using the log-rank (Mantel-Cox) test. p values < 0.05 were considered statistically significant.